Measurements of Plasma Density Fluctuations and Electric Wave Fields using Spherical Electrostatic Probes

Anders I. Eriksson and Rolf Boström

Swedish Institute of Space Physics, Uppsala Division,
S-755 91 Uppsala, Sweden

IRF Scientific Report 220
April 1995

Swedish Institute of Space Physics
Kiruna 1995
ISSN 0284-1703

Digital reprint 2025

This is a 2025 digital reprint of the original report from 1995, created by the first author from the same LaTeX code but with graphics scanned from the original printed version as the digital originals could no longer be found. Inevitable changes of figure sizing and reference formatting resulted in slight changes to line and page breaks, but all figures, equations and section headings are still on the same pages as before. No other intentional additions or differences to the original text have been introduced except on this page.

Contents

Abstract

Spherical electrostatic probes are in wide use for the measurement of electric fields and plasma density. This report concentrates on the measurement of fluctuations of these quantities rather than background values. Potential problems with the technique include the influence of density fluctuations on electric field measurements and vice versa, effects of varying satellite potential, and non-linear rectification in the probe and satellite sheaths. To study the actual importance of these and other possible effects, we simulate the response of the probe-satellite system to various wave phenomena in the plasma by applying approximate analytical as well as numerical methods. We use a set of non-linear probe equations, based on probe characteristics experimentally obtained in space, and therefore essentially independent of any specific probe theory. This approach is very useful since the probe theory for magnetized plasmas is incomplete.

1 Introduction

The literature on the theory of probe measurements is extensive, starting with the work of Langmuir in the 1920s (e.g., *Mott-Smith and Langmuir*, 1926). Recently, there has been some emphasis on the problems occurring in these types of measurements in space plasmas. In particular, the influence of density fluctuations on measurements of electric fields has been theoretically studied by *Diebold et al.* (1994) and *Laakso et al.* (1995), and the effects of rectification of wave signals by nonlinearities in the probe sheaths has been discussed by *Boehm et al.* (1994) with applications to observations from sounding rockets. Here, we will study these and other spurious components in the signals from the probes, emphasizing the use of multiple probe measurements for their identification. We concentrate on the measurements of fluctuations of the electric field and plasma density rather than their background quasi-static values. This approach enables us to use a semi-empirical approach essentially independent of the details of the incompletely known probe theory.

The discussion is illustrated by measurements from the Viking (*Hultqvist*, 1990) and Freja (*Lundin et al.*, 1994) satellites. Both these spacecraft were equipped with a set of spherical probes on wire booms in the spin plane (Table 1). We use data from the instruments V4L on Viking and F4 on Freja (*Holback et al.*, 1994), both measuring several electric wave field and/or density fluctuation signals using the spherical probes. The same sets of probes are also used by the instruments V1 on Viking and F1 on Freja, and additional properties of the probes can be found in descriptions of these instruments (*Block et al.*, 1987; *Marklund et al.*, 1994).

When a probe is used for the measurement of plasma density fluctuations, it is biased to a positive potential V_P with respect to the plasma. Electrons are then attracted and collected by the probe, and under certain conditions (Section 2.1), the collected current I_P will be proportional to the number density of electrons. Ideally, I_P should be insensitive to variations of V_P for this type of measurement, to ensure that fluctuations in the probe current due to variations in the probe potentials are not mistakenly interpreted as density variations. This means that the differential resistance $R = (dI_P/dV_P)^{-1}$ should be as high as possible. The function $I_P(V_P)$ is known as the probe characteristic, its graph being the probe curve. Figure 1 shows examples of probe curves from Viking and Freja, recorded by sweeping the bias potential of a probe (with respect to the satellite) and measuring the current flowing from the satellite body through the probe and out to the plasma. Often, plasma characteristics such as temperature and density are derived from probe sweeps of this type with the aid of some probe theory. This is not the aim of the present study, where we concentrate on studies of fluctuations, as opposed to background parameter values. Our principal use of the experimentally determined probe curve is as a tool for diagnosing measurements of electric field and density fluctuations.

When measuring electric fields (*Fahleson*, 1967; *Mozer*, 1973), two probes are fed with the same bias current I_B, and the voltage between them is measured. If the plasma conditions at the two probes are identical, they follow identical probe curves, and as they are fed with the same I_B, they have the same V_P. Any voltage between the probes therefore is due to electric fields in the plasma. To minimize the error in this technique, I_B should be chosen so as to place the probe at a point on the probe curve where the current-voltage relation depends as little as possible on the conditions in the plasma. If this was perfectly satisfied, the probe would always stay on the same potential with respect to the plasma, and thus the voltage between any two probes would precisely give the voltage variation due to electric fields in the plasma. One should note that even though the voltage measurement would be accurate, the electric field estimate could still be erroneous due to finite wavelength effects.

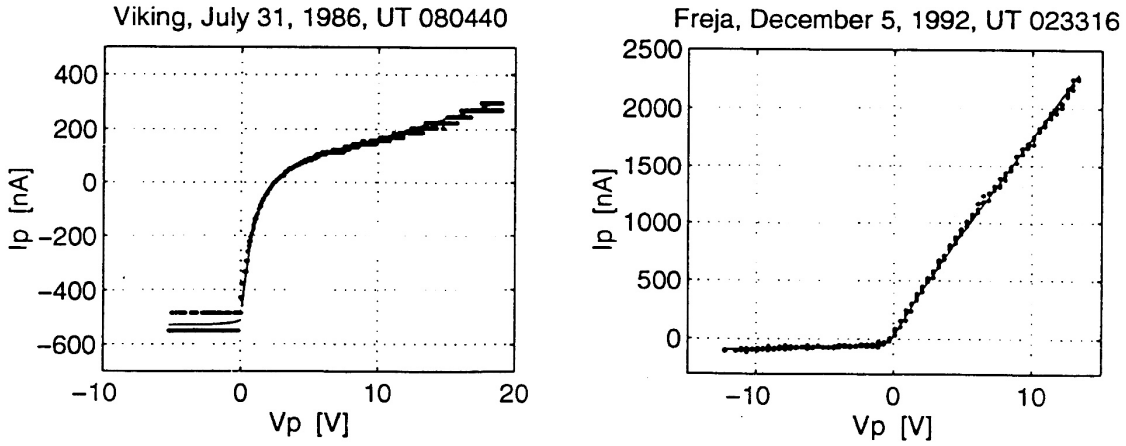

Figure 1: Examples of Langmuir sweeps. Normally used bias values are found in Table 1. The voltage axis has been rescaled by $V_P = V_S + V_B$, where V_S is given below. Dots are measured values, solid lines are parametrizations as in Section 2.3 with the following values: Viking (left): $I_{ph,0} = 530$ nA, $T_{ph} = 1$ eV, $\alpha n = 18$ cm^{-3}, $T^* = 1$ eV, $\beta n = 0$, $V_S = 3$ V. Freja (right): $I_{ph,0} = 50$ nA, $T_{ph} = 1$ eV, $\alpha n = 350$ cm^{-3}, $T^* = 0.4$ eV, $\beta n = 1000$ cm^{-3}, $m^* = 4$ u, $V_S = -1.3$ V.

	Viking	Freja
Total number of spherical probes:	4	6
Number of voltage probes:	2 - 4	2 - 6
Number of density probes:	0 - 2	0 - 4 (P3 - P6)
Probe radius:	5 cm	3 cm
Boom length:	40 m	10.6 m (P1 - P4)
		5.6 m (P5, P6)
Most used bias voltage:	16 V	10 V
Most used bias current:	-150 nA	22 nA
Satellite spin rate:	3 rpm	10 rpm
Typical satellite speed:	3 km/s	7 km/s
Typical measurement altitude:	5,000 - 13,000 km	1700 km
Typical magnetic field:	2 - 9 μT	25 μT
Typical plasma density:	1 - 1,000 cm^{-3}	100 - 5,000 cm^{-3}
Typical electron temperature:	0.5 - 2 eV	0.2 - 0.4 eV
r_P/λ_D:	0.005 - 0.3	0.05 - 1
r_P/r_{ge}:	0.05 - 0.1	0.3 - 1
$\lambda_D/r_{ge} \sim f_{ce}/f_{pe}$:	1 - 10	2 - 10

Table 1: Instrument and plasma parameters for Viking and Freja. Electron temperatures for Viking are derived by fitting of probe curve from OML theory for an unmagnetized plasma to measured probe sweeps. For Freja, a model electron temperature is used (*Brace and Theis*, 1981).

2 Probe theory

2.1 Particle collection by spherical probes: Orbital motion limited or sheath limited

In a sufficiently thin plasma, the screening of the potential field from the probe is weak. The motion of any single charge is then essentially independent of the motion of other charges, and we say that the collection of particles by a probe is orbital motion limited (OML). If the plasma is dense, the field around a probe is significantly influenced by space charge effects and the Debye screening effect of the charged particles around it. The properties of the sheath will change with the collected current, and the theoretical description of probe operations in such circumstances is rather involved. This is the sheath limited (SL) regime of particle collection. The transition between the two cases is given by a comparison of the characteristic dimension of the applied field, which is the probe radius r_p, and the intrinsic screening distance in the plasma, which is the Debye length λ_D. The condition of validity of OML theory thus is

$$r_P \ll \lambda_D. \tag{1}$$

Since the particle motions do not affect the potential in the OML case, it follows that the current carried by plasma particles hitting the probe is proportional to the plasma density. In sunlight, there will also be a current due to the emission of photoelectrons from the probe. Thus, the current to the plasma from a probe at potential V_P with respect to the plasma is

$$I_P = n\,F(V_P, T, ...) + I_{ph}(V_P, ...), \tag{2}$$

where n and T are the number density and the temperature of the collected particle species and the dots indicate other possibly important parameters, the most important of which we expect to be the magnetic field in the plasma and the spacecraft speed, and F is some as yet unspecified function. In this report, we use the convention that currents are positive when flowing from the probe or the spacecraft to the plasma. The photoelectron current can be expected to be of the form

$$I_{ph}(V_P) = \begin{cases} -I_{ph,0}\,\exp(-V_P/T_{ph})\,, & V_P > 0 \\ \\ -I_{ph,0}, & V_P < 0\,, \end{cases} \tag{3}$$

where solar irradiation and probe surface properties determines the constants $I_{ph,0}$ and T_{ph}, and a Boltzmann distribution is assumed[1]. As discussed by *Pedersen* (1995), it is sometimes a better approximation to describe the photoelectrons as a superposition of two Boltzmann distributions with different temperatures. However, for our purposes, equation (3) is sufficient for describing the observed probe characteristics.

Comparing to the sweeps in Figure 1, it is clear that the importance of I_{ph} is much larger in the thin plasma encountered by Viking than in the denser plasma on Freja altitudes. Typically, T_{ph} is a few eV, so for the normally used bias voltages of 10 – 20 volts, the contribution from the photoelectron current is usually negligible. In particular, it can be neglected at the operation points of the density probes (Figure 1), where the probe current then is linear in density (2).

[1]We will here use the convenient convention of refering to T_{ph}, which according to (6) has the dimension of potential, as a temperature in eV. Other temperatures will be treated in a similar fashion, implicitly assuming normalization to Boltzmann's constant and the elementary charge.

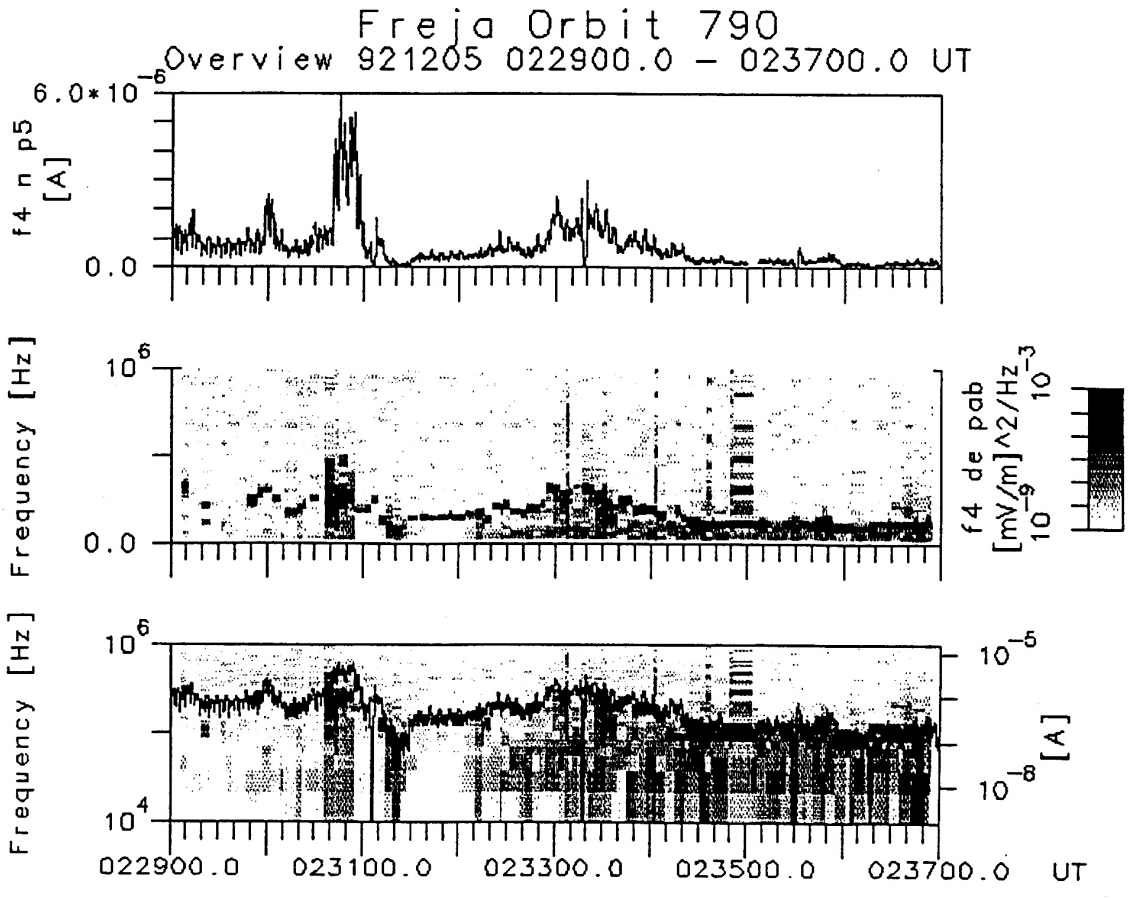

Figure 2: Freja F4 data showing probe current dependence on plasma density. Top: Probe current from probe 5. Center: Spectrogram of high frequency waves. The electron cyclotron frequency f_{ce} is around 800 kHz. Bottom: Superposition of (a) and (b) with suitable logarithmic axis scaling.

Finding the function F in the case of magnetized plasmas is a complicated task, still subject to research in the field of probe theory (*Laframboise and Sonmor*, 1993). However, regardless of F, equation (2) implies that if we can neglect the photoelectron current, the response δI_P of the probe current to fluctuations in the plasma density δn is

$$\frac{\delta I_P}{I_{P0}} = \frac{\delta n}{n_0} \tag{4}$$

if all other parameters are constant. This fundamental result is independent of F, and is valid in all situations where OML theory applies, also in magnetized plasmas.

2.2 Validity of OML theory

Table 1 shows some typical values of r_p/λ_D encountered by Viking and Freja, which may be compared to the criterion of validity for OML theory (1). The conclusion is that the OML approximation normally is applicable, although it may fail in particularly dense plasmas encountered by Freja.

The conclusion that OML applies is supported by experimental verification of an $I_P \propto n$ relation. The upper plot in Figure 2 shows the probe current to probe 5 during part of a Freja orbit, and spectrogram of high frequency waves detected during the same time interval are seen in the center panel. Two interesting features in this spectrogram are narrow band emissions, seen during most of the time interval shown (near 200 kHz at UT 023200, for instance), and an upper cutoff, for example near 450 kHz at 023040. Natural interpretations of these features in the spectra are in terms of Langmuir waves near the plasma frequency f_p, and the upper cutoff of the whistler mode, respectively (see, for instance, Figure 2 of *André* (1985)). As $f_p \propto \sqrt{n}$, it should be possible to have the probe current follow the plasma frequency emissions if we choose scales so as to have a variation by a factor N in current correspond to a factor $\sqrt{N}$ in frequency, if the probe current is linear in the density. The bottom plot shows that this is approximately the case. An extended study of how the probe current depends on plasma density, as determined from plasma frequency emissions, has been made by *Carlson* (1994), who found that the linear relation between I and n suggested by Figure 2 is approximately valid for densities varying over almost two orders of magnitude.

Experimental support for the approximate applicability of the OML approximation is also found in the high degree of linear dependence of the probe current on the voltage found for probe potentials well above zero in the experimentally obtained probe characteristics (Figure 1). In a plasma with strong shielding effects, the probe current would rather be expected to follow the Child-Langmuir 3/2 power law (*Chen*, 1965).

Thus, the deviation of the actually valid probe theory from OML theory cannot be very large. To estimate the errors made by using equation (4), we use numerical results for an unmagnetized plasma by *Laframboise* (1966), assuming that the addition of a magnetic field does not fundamentally change the shielding properties. In his tables 5c and 5f, Laframboise tabulates the probe current as a function of r_P/λ_D for various values of V_P/T_e assuming $T_i = T_e$ and $T_i = 0$, respectively. By the use of cubic spline interpolation on these results, we have calculated the effects of finite λ_D on the validity of (4) for realistic Freja parameters. It can be seen in Figure 3 that the error in the $\delta n/n_0$ estimate is linear in the amplitude for fluctuations up to tens of per cent, and is very small even for density as high as 5,000 cm^{-3}. We conclude that the error introduced into (4) by finite Debye length effects is small in the cases of Viking and Freja, so that the OML relations (2) and (4) hold to good accuracy for these spacecraft.

2.3 Parametrization of probe sweeps

The function nF in (2) is experimentally available from probe bias sweeps. It is often sufficient to describe the essentials of the probe performance by the local properties of the probe curve near the point of operation of a probe. This approach is used in Section 3. However, for making detailed numerical calculations and simulations of the complete probe-spacecraft-plasma system, as we will do in Sections 4.2 and 5.3, it is sometimes useful to parametrize this function. We do this by fitting measured sweeps to an expression

$$I_P(V_P) = I_e(V_P) + I_i(V_P) + I_{ph}(V_P) \tag{5}$$

where I_{ph} is given by (3), and the other terms describe collection of plasma electrons and ions, respectively. For I_e, we use

$$I_e(V_P) = \begin{cases} I_{e0}\,(1 + V_P/T^*)\,, & V_P > 0 \\ \\ I_{e0}\,\exp(V_P/T^*), & V_P < 0, \end{cases} \tag{6}$$

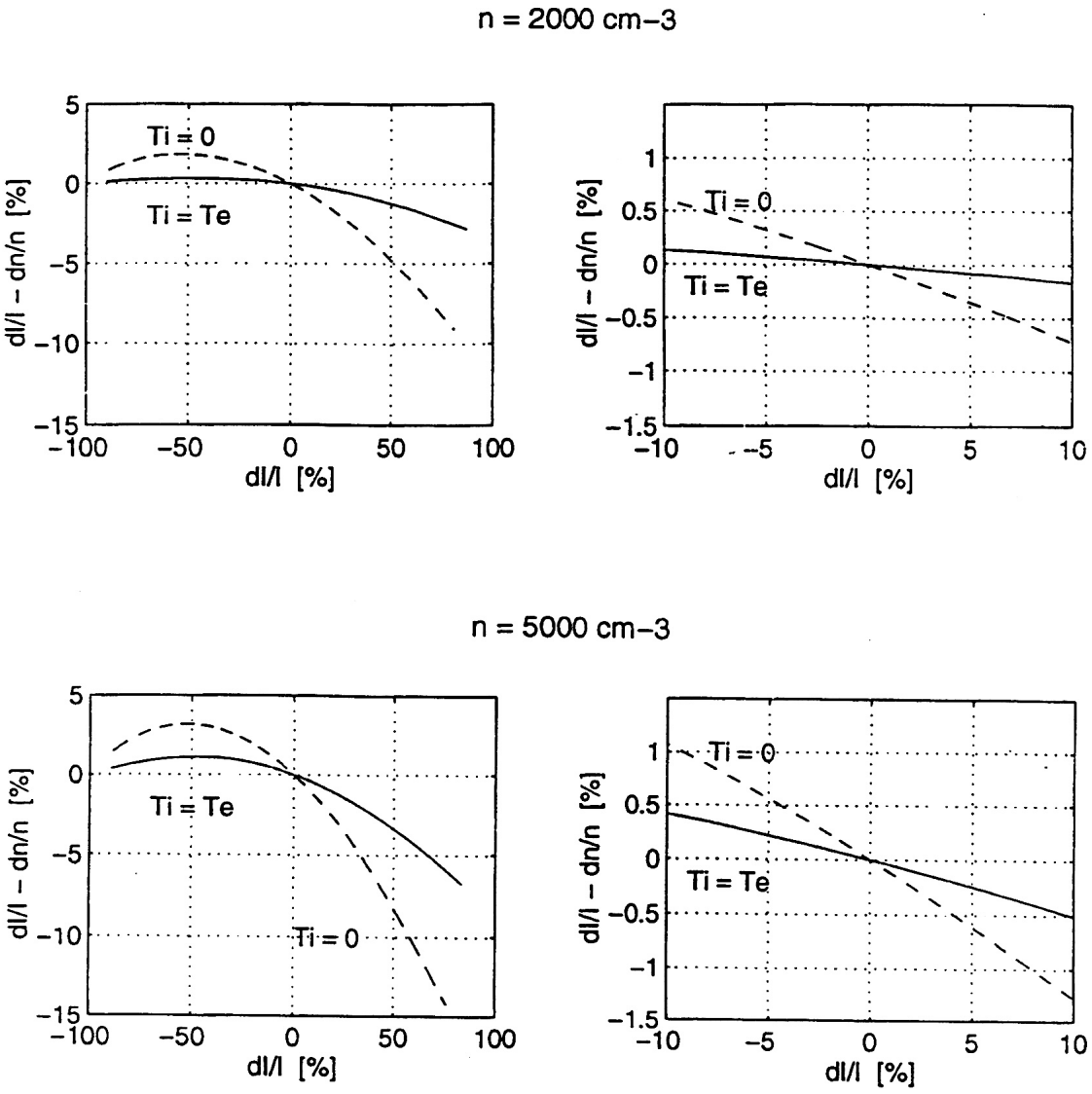

Figure 3: The error, due to finite r_P/λ_D, made when assuming $\delta n/n = \delta i/i$. $T_e = 0.4$ eV, $r_P = 3$ cm, and $V_P = 10$ V has been assumed. Based on numerical results by *Laframboise* (1966).

where

$$I_{e0} = 4\pi r_P^2 e\alpha n \sqrt{\frac{eT^*}{2\pi m_e}} \tag{7}$$

and αn and T^* are parameters of the fit. The form of (6) is inspired by the OML theory for an unmagnetized plasma (*Mott-Smith and Langmuir*, 1926), where this result holds with $\alpha = 1$ and $T^* = KT_e/e$. The conditions of validity for this theory are the OML condition (1) and the two conditions of negligible magnetic field effects,

$$r_P/r_{ge} \ll 1 \tag{8}$$

and (*Rubinstein and Laframboise*, 1982)

$$\lambda_D/r_{ge} \sim f_{ce}/f_{pe} \ll 1, \tag{9}$$

where r_{ge} is the thermal electron gyroradius, and f_{ce} and f_{pe} are the electron cyclotron and plasma frequencies, respectively. Comparing to Table 1, condition (9) is almost always violated on both Viking and Freja, while the other relations generally are satisfied. For Freja, the insufficiency of unmagnetized OML theory has been experimentally demonstrated by *Carlson* (1994) However, in Section 2.1 we concluded that the current of collected electrons is approximately linear in density, so the dimensionless factor α in (6) takes care of effects of magnetization and small deviations from OML conditions on the density dependence of I_e. For the temperature, a "rounding of the knee" effect (*Laframboise and Rubinstein*, 1976; *Rubinstein and Laframboise*, 1982) may cause T^* to be lower than T_e. On the other hand, electron temperature estimates from Langmuir probes are sometimes found to be higher than values derived by other methods (*Carlson and Sayers*, 1970; *Benson et al.*, 1977). These problems are of little concern to us here. Our interest is to get a parametrization of the probe sweeps, and we leave the interpretation of T^* open.

For the current of collected ions, we use a similar modification of known results for an unmagnetized plasma. The ion current will be seen to be negligible in the case of the applications to Viking data. Freja moves at a speed $v_{sat} \approx 7$ km/s, so if the plasma drift can be neglected, the ram energy $\frac{1}{2}m_i v_{sat}^2$, where m_i is the ion mass, is 0.25 eV for H^+ ions and 4 eV for O^+. Normally, the ion temperature T_i can be expected to be below the ram energy, particularly for oxygen, which is usually the dominating ion species. The ion current is then described by (*Fahleson et al.*, 1974)

$$I_i(V_P) = \begin{cases} \pi r_P^2 \beta n e v_{sat} \left(1 - \frac{2eV_P}{m^* v_{sat}^2}\right), & V_P < \frac{m^* v_{sat}^2}{2e} \\ 0, & V_P \geq \frac{m^* v_{sat}^2}{2e} \end{cases} . \tag{10}$$

If the plasma is unmagnetized, $\beta = 1$ and m^* is the effective ion mass, $m^* = m_{eff} \equiv n/\sum_i n_i/m_i$ where the sum runs over ion species. As the gyroradius is much larger for ions than for electrons with corresponding energies, magnetic field effects are expected to be less important for the ions than for the electrons, so $\beta \approx 1$ and $m^* \approx m_{eff}$ may very well hold in the cases to be studied here. In case the ion temperature is higher than the ram energy, the ion current will have a form similar to the electron current in (6), and its functional dependence on V_P and n will therefore be the same for negative probe potentials, which is the only region where I_i is an important part of the total probe current. Hence, it should be possible to fit observed probe sweeps to (10) under quite general circumstances, even though the value of β and m^* may be very different from 1 and m_{eff}. Again, this is of no concern to us, since our goal is to find an empirical parametrization of the probe curve, not to establish its actual dependence on physical parameters.

In Figure 1, we find examples of fits of the parameters αn, T^*, βn, and m^* to observed current-voltage characteristics. For the shown Viking sweep, it is evident that the photoelectron current (3) dominates over the ion current (10), which hence has been put to zero.

3 Probe response to fluctuations in density and electric field

3.1 Resistive coupling

Assuming all other parameters to be constant, the probe current response to arbitrarily large density fluctuations δn and small potential perturbations δV_P is found from equation (2) to be

$$\frac{\delta I_P}{I_{P0}} = \frac{\delta n}{n_0} + \frac{1}{I_{P0}} \left(\left[n \frac{\partial F}{\partial V_P} + \frac{\partial I_{ph}}{\partial V_P} \right] \delta V_P + \frac{1}{2} \left[n \frac{\partial^2 F}{\partial V_P^2} + \frac{\partial^2 I_{ph}}{\partial V_P^2} \right] (\delta V_P)^2 + ... \right) = \\ = \frac{\delta n}{n_0} + \frac{\delta V_P}{R I_{P0}} + a_2 (\delta V_P)^2 + ... \tag{11}$$

From experimentally obtained probe characteristics, we may calculate the probe sheath resistance,

$$R = \left(\frac{\partial I_P}{\partial V_P} \right)^{-1}, \tag{12}$$

as well as a measure of the local nonlinearity of the probe curve near the operation point of the probe,

$$a_2 = \frac{1}{2 I_P} \frac{\partial^2 I_P}{\partial V_P^2}. \tag{13}$$

As is seen in Figure 1, I_P is almost linear in V_P for several volts around the point of operation of the density probes, and a_2 and higher nonlinearities may often be neglected. For voltage probes, a_2 may be larger, and the validity of the expansion (11) is more restricted. Effects of the nonlinearity will be treated in Section 5.

The neglect of fluctuations of other parameters than density and electric field normally is a constraint only on temperature fluctuations. Magnetic wave fields are in all applications to the ionosphere and inner magnetosphere much smaller than the ambient geomagnetic field, and their effect can safely be neglected. Changes in the distribution functions of the collected particle species can take place on short spatial scales. The density and temperature, being the first and third moments of the distribution function, take care of the most important of these. The second moment, the drift velocity, is generally not very important to the probe current, unless the fluctuations are very large. Therefore, the most serious constraint on the equations above is that the fluctuations should be isothermal. The ion current to the biased probes is usually negligible, in particular for density probes, so the restriction to isothermal conditions is mainly on the electrons. For many wave phenomena, it is reasonable to assume $\delta T/T \ll \delta n/n_0$, although wave structures with trapped electrons may violate this assumption. For spatial structures, $\delta T/T$ may be large. The effect of fluctuating electron temperature may be estimated by use of OML theory for an unmagnetized plasma. From equation (6) with $T^* = T_e$, it follows that the probe current response is

$$\frac{\delta I_P}{I_{P0}} = \frac{1}{2} \frac{1 - V_P/T_e}{1 + V_P/T_e} \frac{\delta T_e}{T_e}. \tag{14}$$

For density probes, we usually have $V_P \gg T_e$, and then get $\delta I_P/I_{P0} \sim (1/2)\delta T_e/T_e$. For the voltage probes on Viking, V_P is a few volts positive. Therefore, V_P will often be close to the ideal value T_e which removes the sensitivity to temperature fluctuations. For the voltage probes on Freja, the 22 nA bias current places V_P close to zero, and the coefficient in front of $\delta T_e/T_e$ in (14) is therefore sensitive to variations in V_P.

3.2 Capacitive coupling

The resistive coupling between probe and plasma, described by (11) dominates for low frequency perturbations. For higher frequencies, a capacitive term must be added to the probe current. If C_P is the capacitance of the probe to the plasma, we have

$$I_P = n\,F(V_P, T, ...) + I_{ph}(V_P, ...) + C_P \frac{dV_P}{dt}. \tag{15}$$

Equation (11) is then generalized to

$$\frac{\delta I_P}{I_{P0}} = \frac{\delta n}{n_0} + \left(\frac{1}{RI_{P0}} + \frac{C_P}{I_{P0}} \frac{d}{dt} \right) \delta V_P + a_2 \left(\delta V_P\right)^2 + ... \tag{16}$$

Finding a theoretical estimate of the probe capacitance is a non-trivial problem. For the limit of small probe potential, $V_P \ll T$, the potential around the probe is in the unmagnetized case described by the Debye shielding law, which with boundary conditions relevant for a sphere of radius r_P reads

$$V(r) = \frac{Q}{4\pi\epsilon_0} \frac{\lambda_D}{\lambda_D + r_P} \frac{e^{(r_P - r)/\lambda_D}}{r}, \tag{17}$$

where Q is the charge on the probe. In that case, the capacitance of the probe to infinity is

$$C_D \equiv \frac{Q}{V(r_P)} \equiv \frac{Q}{V_P} = 4\pi\epsilon_0 r_P \left(1 + \frac{r_P}{\lambda_D}\right) = C_0 \left(1 + \frac{r_P}{\lambda_D}\right), \tag{18}$$

where C_0 is the capacitance in vacuum. One may note that this coincides with the expression for the capacitance of the probe to an outer concentric sphere of radius $r_P + \lambda_D$.

In practice, density probes are usually biased to values $V_P \gg T_e$, violating the assumption behind the Debye law. However, the result (18) is still of interest as it shows that for $\lambda_D \lesssim r_P$, the probe capacitance can depend strongly on the local plasma properties. For sunlit probes, the situation is complicated by the presence of a photoelectron sheath around the probes. The current through the sheath may also change the potential distribution around the probe, which affects the capacitance. We also know that the dielectric properties of a plasma vary with frequency and wavelength of the perturbation, as described by the dielectric function (dielectric tensor) of the plasma, and the capacitance may thus vary with frequency. However, in simulations by *Calder and Laframboise* (1985) for a sphere of radius $r_P = \lambda_D$ in an unmagnetized plasma, such effects were apparent only above about half the plasma frequency. Finally, magnetization effects may have a significant impact on the shielding properties of a current carrying plasma, and thereby on the capacitance. It is not possible to explore these issues in this study, where we will assume that the displacement current $C_P\ dV_P/dt$ is well described by a constant capacitance C_P. This assumption will be seen to work well in the applications to Viking and Freja observations below, although we will have reason to discuss it again in section 5.3.3.

For Freja, we may use experimental results by *Lindqvist et al.* (1994), who investigated the relaxation of the probe potential after steplike variations in bias current. They found that the capacitance of a probe at $V_P \approx 8$ V was $C_P \approx 14$ pF. As $C_0 = 3.3$ pF for the Freja probes, this is far above what is predicted by (18), indicating the importance of one or several of the effects listed above.

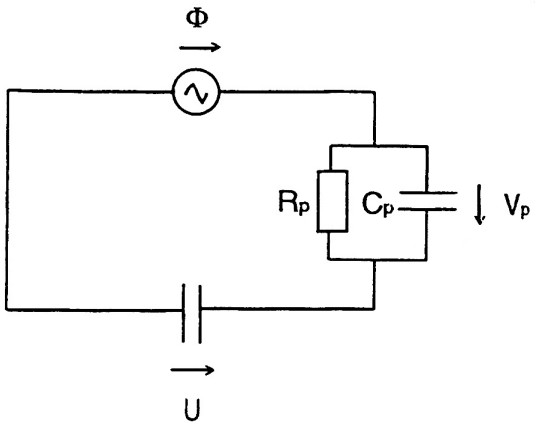

Figure 4: Simple circuit description of instrument response to AC signals when in voltage mode.

3.3 Influence from instrument electronics

The probe current passes the instrument electronics, the input impedance of which therefore must be considered. In current mode (density measurements), the input resistance of the electronics is a few tens of ohms, and the input capacitance ~ 10 pF, yielding an RC time constant on the nanosecond scale. The capacitance can therefore always be neglected. Since the resistance of the probe sheath is above 1 MΩ, we can safely neglect the input resistance as well. In voltage mode (electric field measurements), the input resistance is of the 100 GΩ order, while the input capacitance C_E is 15 pF for Viking, 2.5 pF for Freja probes 1 and 2, and 6 pF for the remaining Freja probes 3 to 6. Hence, the RC time of the electronics is on the tenths of seconds scale, so for all wave measurements, effects of the input resistance are negligible. However, C_E is of the same order of magnitude as C_P (Section 3.2) and cannot be neglected.

In the simplest assumption, where the spacecraft body is seen as a ground for time-varying electric signals, the probe sheath and the electronics in the probe constitute a circuit. For small amplitude perturbations, we may linearize and represent the circuit as in Figure 4 (more complete and nonlinear circuit models will be introduced in Section 4.1). In this model, the measured probe voltage δU is coupled to the applied voltage variation in the plasma $\delta\Phi$ by

$$\left[(C_E + C_P)\frac{d}{dt} + \frac{1}{R}\right]\delta U = \left[C_P\frac{d}{dt} + \frac{1}{R}\right]\delta\Phi \tag{19}$$

with solution

$$\delta U = e^{-t/R(C_P+C_E)} \int^t e^{t/R(C_P+C_E)} \left(\frac{1}{1+C_E/C_P}\frac{d}{dt} + \frac{1}{R(C_P+C_E)}\right)\delta\Phi\, dt. \tag{20}$$

For frequencies $f \ll f_C = \frac{1}{2\pi R(C_E+C_P)}$ the resistive terms dominate, and $\delta U = \delta\Phi$. For frequencies $f \gg f_C$ the capacitive terms are dominating, and we have $\delta U = C_P\,(C_E + C_P)^{-1}\,\delta\Phi$.

3.4 Application: Freja observations of high amplitude waves in the lower hybrid frequency range

André et al. (1994) and *Eliasson et al.* (1994) studied an event with high amplitude waves in the

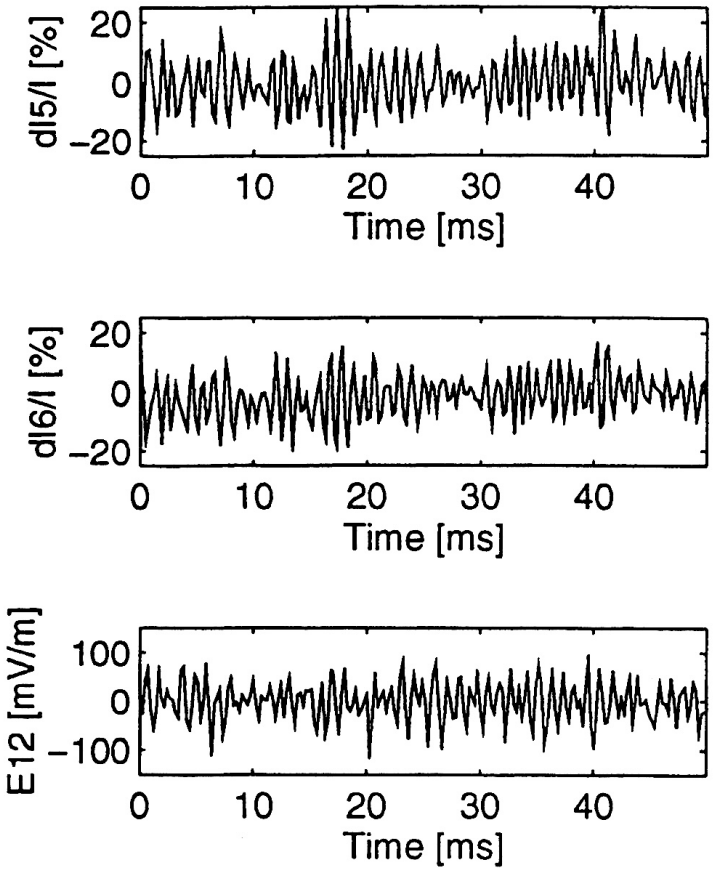

Figure 5: Time series of electric field (bottom) and probe current fluctuations to probe 5 (top) and 6 (center) recorded by the F4 instrument on Freja on December 5, 1992, Freja orbit 790. Time axis starts at UT 023519.9.

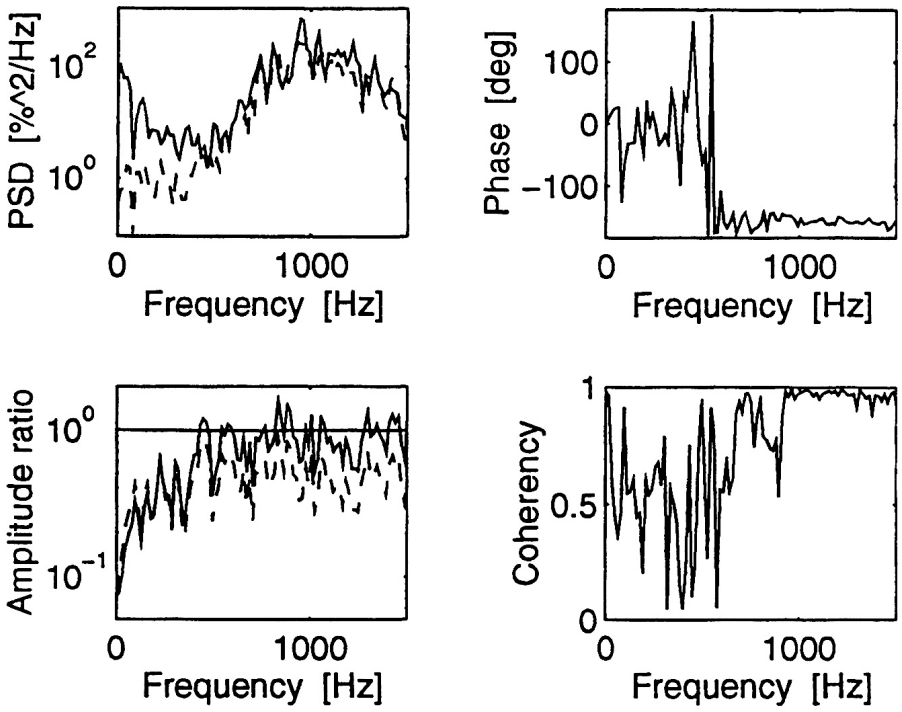

Figure 6: Spectral analysis of the data partly shown in Figure 5. The different plots are discussed in Section 3.4.

lower hybrid frequency range coincident with strong transverse ion energization. Part of the time series of these signals is shown in Figure 5. The strong high-frequency fluctuations in the probe currents as well as their resemblance to the electric field signals suggests that the $\delta I_P/I_{P0}$ signals are dominated by effects of probe voltage variations rather than by density fluctuations. This is consistent with the cross spectral analysis of the two probe current fluctuation signals seen in the two right panels of Figure 6 (for discussions of the application of cross spectral techniques to probe measurements in space we refer to reports by *LaBelle and Kintner* (1989); *Holmgren and Kintner* (1990); *Vago et al.* (1992)). The bottom panel shows the coherency between the two signals. High coherency is found mainly above about 500 Hz. However, for a coherent density fluctuation, the relative phase ϕ between the probe signals should vary with frequency f so that $2\,\pi\,df/d\phi$ times the probe separation is the Doppler shifted (by the spacecraft motion) phase velocity of the density perturbation in the direction of the probe separation. The relative phase is shown in the upper right plot, and it is seen that the two probe current signals are approximately 180 degrees out of phase in the region of high coherency. As the two probes are mounted on opposite sides of the satellite, a long-wavelength external electric field will increase the potential of probe 5 when it decreases the potential of probe 6. According to (16), the observed 180° phase shift is therefore qualitatively explained by the influence of the wave electric field on the probe currents. We now turn to a quantitative analysis.

Figure 7 shows the configuration of the Freja antennas at UT 023520, viewed along the geomagnetic field $\mathbf{B}_0$. A nearby probe sweep (not shown) yields $R = 55$ MΩ and $I_{P0} \approx 205$ nA at $V_B = 16$ V. The transition between resistive and capacitive coupling therefore is at $f_C = 1.3$ kHz.

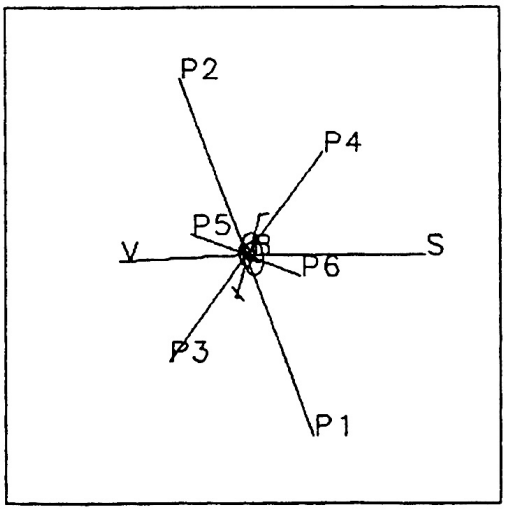

Figure 7: The probe configuration of Freja at UT 023520, December 5, 1992, as viewed along the geomagnetic field. The spacecraft velocity is in the direction marked V, while S denotes the direction to the sun.

Comparing to the spectrum in the upper left plot of Figure 6, we have to include resistive as well as capacitive coupling by using (19) on the measured voltage to get the real potential variations in the plasma. Assuming that the wave electric field is predominantly in the direction perpendicular to $\mathbf{B}_0$, we may calculate the voltage variations on probes 5 and 6 due to the observed electric field. In this case, only one electric field component, E_{12}, is measured, so it is not possible to exactly construct the relevant potential variations. However, for these broad-band waves, it is not unreasonable to assume that the power of the electric wave field is approximately the same in all directions when averaged over many wave periods. Hence, it should be possible to construct an almost correct spectrum of the real voltage fluctuations of probes 5 and 6. This would lead to erroneous results only if the electric field is almost linearly polarized and close to the direction of one of the antennas on all frequencies, which is very unlikely for these high-amplitude waves. One may note that the observed amplitudes of $E \approx 100$ mV/m (Figure 5) and plasma frequency 100 kHz (Figure 2) implies a value of the turbulence parameter as high as $W = \frac{1}{4}\epsilon_0 E^2/nKT \sim 10^{-3}$ for the reasonable assumption $T = 1$ eV. This indicates that nonlinear interactions are important for the dynamics of the waves, making the situation of linear frequency-independent polarization unlikely.

If the signal in E_{12} is due to a perpendicular field, this perpendicular field is $E_{12}/\sin\theta_{12}$, where θ_{12} is the angle between the antenna and the magnetic field. We should also correct this field for the effects of capacitive coupling by using (19). According to what we said above, we approximate the projection of the perpendicular wave field in the direction of the booms on which probes 5 and 6 are mounted by $E_{56} = E_{12}\sin\theta_{56}\,/\sin\theta_{12}$. The potential variations on probes 5 and 6 due to this field are found by multiplying by the boom length for these probes, which is 5.5 m. This gives us an estimate of the signal δV_P in (16). As we obtained R and I_{P0} from the probe sweep, all parameters in (16) and (19) are known, and we can calculate the expected probe current variations. As we expect the calculated voltage on the probes to be correct only in a statistical sense, we compare spectra rather than the signals themselves. The solid line in the upper left panel of Figure 6 is the spectrum of measured probe current fluctuations, and the dashed curve is the values predicted from

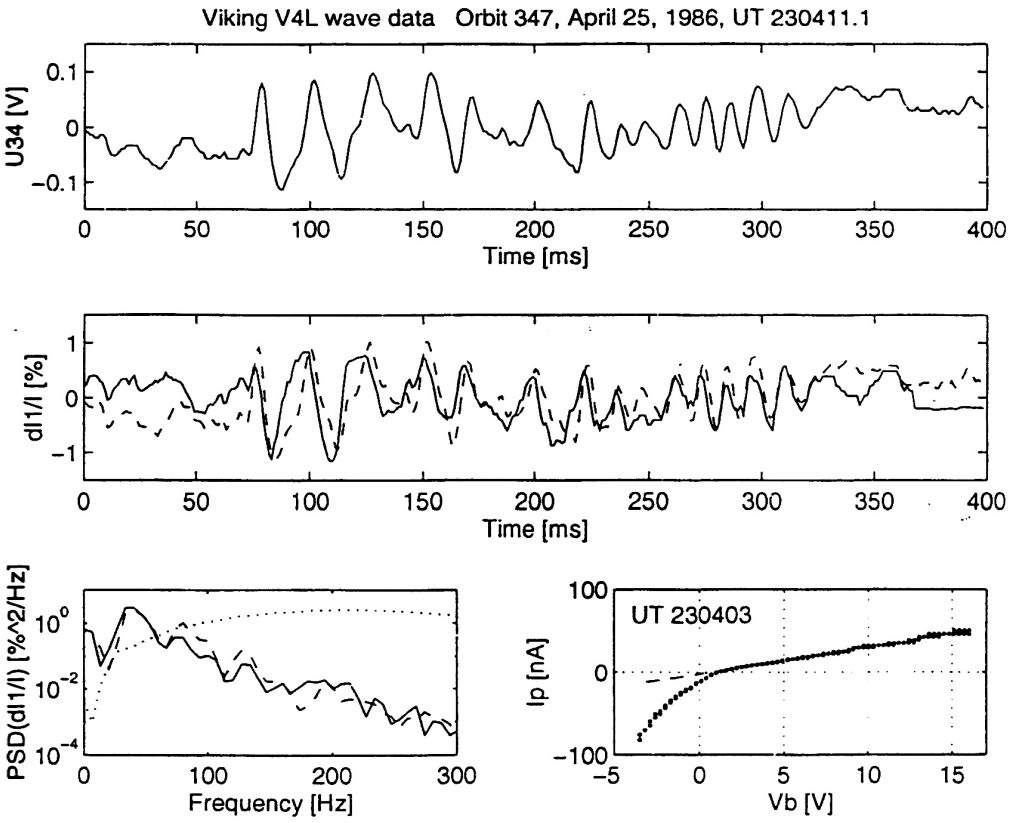

Figure 8: Electrostatic ion cyclotron waves observed by Viking, as discussed in Section 3.5.

(16). The agreement is very good in all the region where the relative phase of the two probe current fluctuations is 180°. To better illustrate this, the ratio of the amplitude spectrum (square root of PSD) of the current fluctuation calculated from the electric field and the corresponding quantity for the measured current is plotted as a solid line in the lower left panel. It is seen that above some 500 Hz, the ratio is close to 1. We thus not only have a qualitative but also a quantitative understanding of the effects of electric fields on the probe current.

This can also be seen as a support for the capacitance value derived by *Lindqvist et al.* (1994). The dashed curve in the lower left panel of Figure 6 shows the result of using the vacuum value of the probe capacitance to infinity, 3.3 pF, instead of the experimentally derived 14 pF. In this case, it is not possible to reproduce the observed probe current fluctuation from the electric field. Calculating the logarithmic mean of the two spectral ratios in the plot for frequencies between 500 and 700 Hz, we get 0.85 for $C_P = 14$ pF and 0.47 for 3.3 pF. To get a spectral ratio of 1, the capacitance should be 17 pF. Of course, there are uncertainties in this method as well as in the method used by Lindqvist et al., but the fact that the results agree to within 20 % indicates that the estimated capacitance is approximately correct.

3.5 Application: Viking observations of electrostatic ion cyclotron waves

Electrostatic (hydrogen) ion cyclotron waves are often observed on Viking (*André et al.*, 1987; *Boström et al.*, 1987), and sometimes also ion cyclotron harmonic waves (*Koskinen et al.*, 1987).

Figure 8 shows an interval of Viking data in a region where the proton cyclotron frequency $f_{cp} = 40$ Hz. In the top panel, which shows the voltage between probes 3 and 4, an oscillation around f_{cp} is seen from about 50 to 250 ms in the plot, and another emission near 2 f_{cp} is visible between 270 and 320 ms. Similar emissions are also seen in the probe current to probe 1, which is shown as the solid curve in the center plot.

The lower right plot in Figure 8 shows a probe sweep recorded close to the wave emissions. From a least squares fit to the linear part of the probe curve (shown as a dashed line), the sheath resistance for the density probes is found to be 310 MΩ. The plasma has very low density (~ 1 cm^{-3}), and the satellite potential is therefore so high that the photoelectron saturation current is never reached in the sweep. For the calculation of the sheath resistance for the voltage probes, we therefore use values $I_{ph,0} \approx 600$ nA and $T_{ph} \approx 2$ eV obtained from a sweep earlier on the same orbit. Due to the low density, the photoelectron current will dominate the current at the point of operation of the voltage probes, and we can calculate the resistance to be a few MΩ. Assuming C_P to be on the order of 10 pF (the vacuum value C_0 is 6 pF), the characteristic frequency f_C is above 1 kHz. The voltage probes are therefore purely resistively coupled to the plasma in this case. For the density probes, $C_P = 10$ pF yields $f_C \approx 50$ Hz, so for these, the capacitive term in (16) must be included.

In this case, the magnetic field was only 11 degrees out of the spin plane, so the method we used in Section 3.4 above to calculate the voltage variation on one probe from a measured signal on another probe pair should be useful. The boom angles with respect to the magnetic field was 74° for probe 1, which was in density mode, and 159 degrees for the probe pair 3 and 4 in voltage mode. Calculating the voltage variations and applying (16), we get an expected probe current fluctuation which is shown as a dashed curve in the center panel. The correspondence between the two curves in this panel is remarkably good. We have here used the resistance from the sweep, $R = 310$ MΩ, and the vacuum capacitance $C_P = 6$ pF. The lower left plot shows the spectra of the measured (solid) and calculated (dashed) probe current fluctuations. The dotted curve shows the ratio of the displacement current to the conduction current.

It is interesting to note that the vacuum capacitance of the sphere to infinity is a good approximation, as this contrasts to the results from Freja discussed above. Studying spectral ratios as in Section 3.4, we find that using the vacuum capacitance and $R = 310$ MΩ from the nearby sweep, the average spectral ratio between 30 and 150 Hz is around 1.1, which we consider to be a very good value. Increasing C_P to twice the vacuum value, the average spectral ratio increases to 1.8. Hence, the capacitance cannot be much above its vaccum value. *Lindqvist et al.* (1994) attributed the high C_P value they found on Freja to the photoelectron sheath. The finding that the vacuum capacitance is a good approximation for the Viking probes cannot be explained within this hypothesis, as the probes were sunlit in both the Freja and Viking cases. The Viking example discussed above was from a region of very low plasma density, so one would rather expect the influence of photoelectrons to be more pronounced in this case. The most striking difference between the Viking and Freja observations instead are that the density is much higher in the Freja case, suggesting that the high C_P value found on Freja has to do with the properties of the natural plasma rather than the photoelectron cloud. An extensive investigation of the different behaviour of the probe capacitance to the plasma on Viking and Freja would clearly be of interest, as well as an extended comparison of results of capacitance estimates by the methods presented above and by *Lindqvist et al.* (1994)

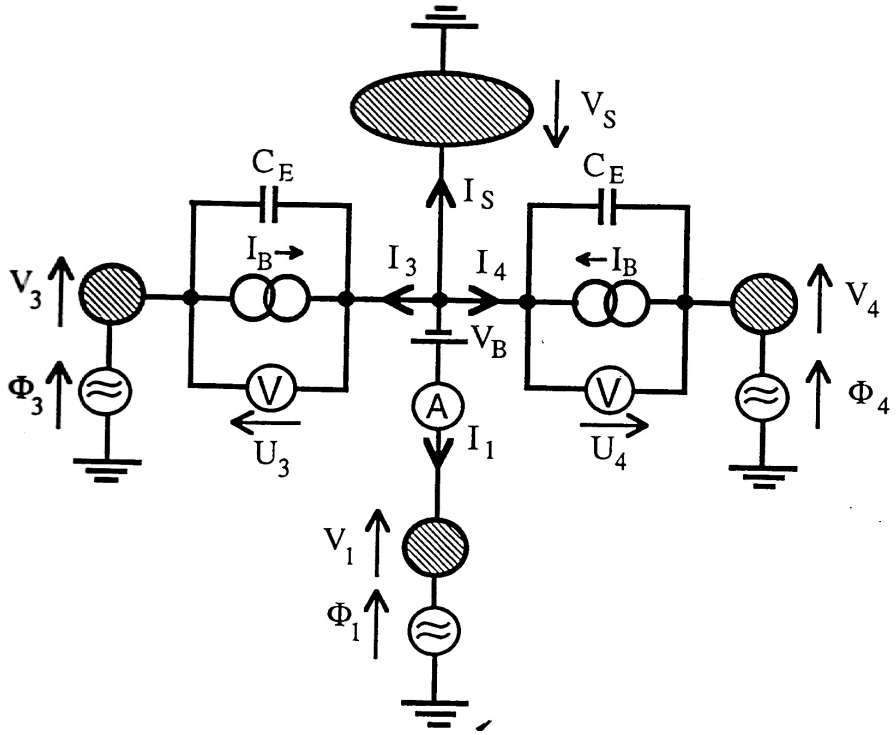

Figure 9: Circuit description of a probe-spacecraft-plasma system.

4 Cross talk and variations in satellite potential

4.1 Circuit description

The currents which flow to the plasma from the probe have to close through the spacecraft body, which itself may be seen as a probe, obeying some current-voltage relationship $I_S(V_S)$, where I_S is the current from spacecraft body to the plasma and V_S is the satellite potential with respect to the plasma. The probe, spacecraft, and plasma form an electric circuit, for which

$$V_S + U_P - V_P - \Phi_P = 0, \tag{21}$$

where U_P is the voltage between probe and spacecraft body, V_P is the potential of the probe relative to the local plasma, and Φ_P is the potential difference between the location of the probe and the spacecraft due to electric fields in the plasma. Assuming that no other instruments complicate the situation, the satellite potential V_S will be determined by the current continuity equation

$$I_S(V_S) + \sum_{P=1}^{N} I_P(V_P) = 0 \tag{22}$$

where N is the total number of probes.

An example of a spacecraft-probe-plasma circuit is shown in Figure 9, depicting a case where two probes (labelled 3 and 4) are in voltage mode (electric field measurements) and one probe is in density mode (probe 1). The sheaths around probes and spacecraft are depicted by shaded ovals in

the circuit. Probes in voltage mode are fed with a bias current I_B. The current from these probes to the plasma is given by

$$I_P(V_P) = I_B - C_E \frac{dU_P}{dt}, \tag{23}$$

where C_E is the input capacitance of the electronics, which according to Section 3.3 is the only instrumental parameter we have to include. Probes in density mode are put at a bias potential, so for these probes

$$U_P = V_B. \tag{24}$$

In a probe instrument, the measured quantities are U_P for voltage probes and I_P for density probes. The equations above form a system of first order ordinary differential equations for how these quantities depend on the space plasma and the electric fields in it. Variations of the plasma parameters enter the system through the dependence of I_P and I_S on these parameters, while the electric field in the plasma is explicitly included through Φ_P. As the equations are coupled, it follows that a perturbation at one probe can give effects for currents to and potentials of the other probes or the spacecraft body. This is what is known as "cross talk". The most important of these effects are the results of varying satellite potential.

If the functions $I_P(V_P)$ and $I_S(V_S)$ are known, the relations above completely describe the probe-spacecraft-plasma circuit. For the probe current, we get direct information from the probe sweeps (Figure 1). To describe I_S, we assume that the spacecraft body can be seen as a spherical probe of radius $r_S = D\, r_P$. We also assume that the currents of collected as well as photoemitted particles scales with area, so that the DC current-voltage relation scales as D^2. For the capacitance, we assume scaling by radius. With these assumptions, (15) translates to

$$I_S(V_S) = D^2\, n\, F(V_S, T, ...) + D^2\, I_{ph}(V_S, ...) + D\, C_P\, \frac{dV_S}{dt}. \tag{25}$$

This scaling should be approximately appropriate in the limit of infinite Debye length. This approximation is not always applicable to the satellite sheath. With $D \sim 15$, we find from Table 1 that $r_S/\lambda_D \ll 1$ can be expected to hold only in tenuous plasmas encountered by Viking. For other cases, in particular on Freja, finite λ_D effects can be expected to be important. Such non-OML effects (Section 2.2) increase both the resistance and the capacitance. Therefore, they are expected to affect the first and last terms of (25) in opposite ways. A deeper analysis of this problem cannot be accomodated in the present work, but we note that in the cases where one of the terms in (25) is dominating, it is likely to do so even if effects of finite r_S/λ_D are included. In such cases, the scaling indicated by (25) may retain an approximate validity with values of D deviating from what is expected from simple geometrical considerations.

Eliminating U_P by using (21), the equations (22) - (24) for a total number of N probes is a system of $N+1$ equations for $N+1$ unknowns (V_S and V_P). The functions $I_P(V_P)$ and $I_S(V_S)$ are assumed to be known from (15) and (25). Input to these equations are the potential differences in the plasma Φ_P and the relative density fluctuations $\delta n_P/n_0$ at the locations of the probes and the spacecraft ($P = S$). The output should be formulated in terms of the quantities really measured on a spacecraft, which usually are the voltages between two probes P and Q,

$$U_{PQ} = \Phi_P - \Phi_Q + V_P - V_Q, \tag{26}$$

or the relative probe current fluctuation, which is

$$\frac{\delta I_P}{I_{P0}} = \frac{I_P(V_{P0} + \delta V_P) - I_P(V_{P0})}{I_{P0}} \tag{27}$$

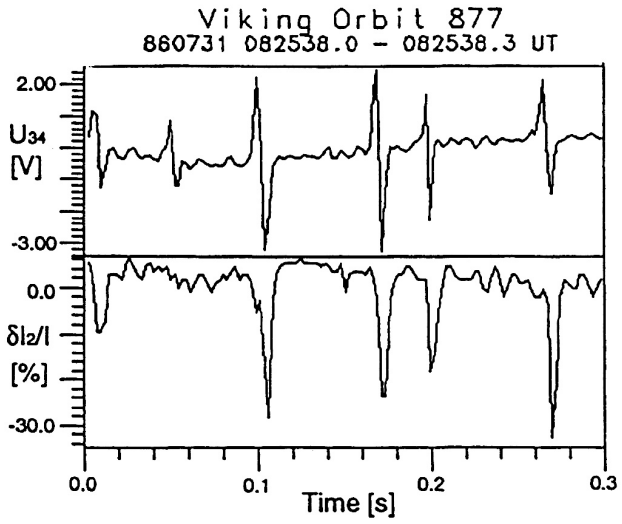

Figure 10: Example of Viking observations of solitary waves.

where I_P from (15) is used. The bias voltage on a density probe is usually sufficiently high to allow the neglect of the nonlinear photoelectron and ion terms in I_e. Equation (27) then reduces to

$$\frac{\delta I_P}{I_{P0}} = \frac{\delta n_P}{n_0} - \frac{1}{V_{P0}} \left[\Phi_P + \frac{RC_P}{1+\delta n_P/n_0} \frac{d}{dt}(\Phi_P + V_S) \right]. \tag{28}$$

In the ideal case, we should have $U_{PQ} = \Phi_P - \Phi_Q$ and $\delta I_P/I_{P0} = \delta n_P/n_0$. However, equations (26) and (28) show that other terms also affect the measurements. The fluctuations in current depend on the potential differences in the plasma and on the variation of the satellite potential, and thus on $\delta n_S/n_0$, as well as on $\delta n_1/n_0$. Likewise, the voltage measurement is influenced by the difference between the potentials of the probes, which reflects differences in the probe sheaths. Thus, different plasma densities at the probes may affect the voltage estimate, as has been discussed by e. g. *Laakso et al.* [1994]. To find the detailed dependence of the measured quantities on the fields $\delta n/n_0$ and Φ, we have to solve the system of equations (22) - (24), and then use (26) and (28).

4.2 Application: Viking observations of solitary waves

Solitary waves (SWs) in the auroral regions at altitudes between 5,000 to 13,000 km have been observed by the S3-3 (*Temerin et al.*, 1982) and Viking (*Boström et al.*, 1988) satellites. For the most recent observational results on these phenomena, the reader is refered to the work by *Mälkki et al.* (1993), *Mälkki* (1993), *Eriksson et al.* (1995) and references therein. The SWs show very high amplitude ($\delta I_P/I_{P0} \lesssim 50$ %). To evaluate the accuracy of the measurements, it is necessary to do a detailed study of the response of the probe-spacecraft-plasma system to these structures. The examples we will show here are also included in the paper by *Eriksson et al.* [1995], which also contains some idealized cases.

An example of Viking SW observations is shown in Figure 10. To simulate the measurements, we assume a plasma with uniform background electron number density n_0 and no background electric field. An electrostatic solitary wave is a localized density depletion with negative potential travelling antiparallel (in the northern hemisphere) to the ambient magnetic field. We let the z

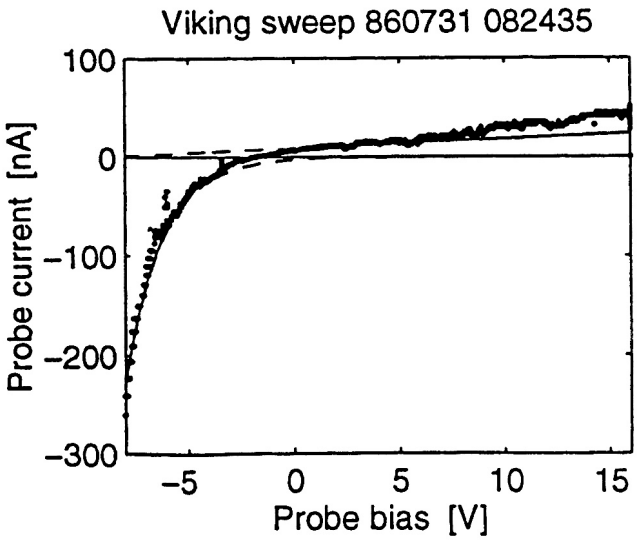

Figure 11: Viking (orbit 877) Langmuir probe sweep inside a SW region, obtained just before the data in Figure 10 (MLT 3.0, MLAT 81.1°, altitude 8965 km). The sweep is parametrized as in Figure 1 with $\alpha n = 0.5$ cm^{-3}, $T^* = 0.2$ eV, $I_{ph,0} = 530$ nA, $T_{ph} = 1.8$ eV, $\beta n = 0$, and $V_S = 9.5$ V.

axis be antiparallel to B. The SW propagates along this axis with speed u, and is assumed to have infinite extent in the perpendicular directions. A symmetric SW could be described by for instance a Gaussian, a hyperbolic secant function, or any other localized function of reasonable appearance. Some of the observed SWs also show a net potential drop over the structure, and are then known as weak double layers (WDLs). To represent these, we may add an inverse tangent, a hyperbolic tangent or some other step-like function to the SW. We model the SW density perturbation by

$$\frac{\delta n(z,t)}{n_0} = -\nu_0 \exp\left(-\left[\frac{z-ut}{L}\right]^2\right), \tag{29}$$

and the potential by

$$\Phi(z,t) = -\Phi_0 \exp\left(-\left[\frac{z-ut}{L}\right]^2\right) - \frac{\Delta\Phi}{2}\tanh\left(\frac{z-ut}{L'}\right). \tag{30}$$

Here ν_0 and Φ_0 are known as the amplitudes of the SWs in relative density fluctuation and voltage, and $\Delta\Phi$ is the net potential drop. The scale length L of the potential well may be estimated from measurements, while the choice of scale length L' over which the net potential drop is distributed is more uncertain.

Choosing coordinates so that the satellite is at $z = 0$, the voltage difference (due to electric fields in the plasma) between the locations of the spacecraft body and any probe $P = 1$, 2, 3, or 4 is $\Phi_P(t) = \Phi(z_P, t) - \Phi(0, t)$, where z_P is the location of the probe. The relative density depletion at a probe ($P = 1$, 2, 3, 4) or at the satellite ($P = S$) is $\delta n_P(t)/n_0 = \delta n(z_P, t)/n$.

The relevant parameters describing the probe characteristic are found by fitting the expressions in Section 2.3 to a nearby probe sweep (Figure 11). Since the probe does not reach photoelectron saturation in this case, the value for I_{ph} is taken from the sweep in Figure 1. We do not expect

the photoelectron properties to change in the 20 minutes which separate these two sweeps. It is therefore surprising to find a different value of T_{ph}. This is probably an artefact due to changing satellite potential during the sweep. In this case the plasma is very tenuous, as is witnessed by the low probe current of 40 nA at 16 V bias potential. To close the bias current of two times -150 nA to probes 3 and 4, the satellite must be at positive potential. When the bias voltage on the density probe is lowered from its normal 16 V during the sweep, the associated probe current also decreases, and the satellite potential has to increase to close the current. This change of V_S causes an apparent increase in T_{ph} when we try to do a fit which assumes constant satellite potential. We therefore use T_{ph} and $I_{ph,0}$ from the sweep in Figure 1 in the following. It should be noted that the probe curve in Figure 11 is not perfectly linear in this case. This is due to an effect of collection of photoelectrons emitted by the boom and the spacecraft, which is seen in very tenuous plasmas when the boom is close to parallel to the ambient magnetic field (*Hilgers et al.*, 1992). Due to the satellite spin, this happens to be the case in the right part of the probe curve in Figure 11. The increased probe current above approximately 10 V is therefore interpreted as due to collection of boom emitted photoelectrons.

For simulation of the measurements, we will study a configuration of Viking with two probes (1 and 2) in density mode and the other probes 3 and 4 in voltage mode. Probe 1 is then at a fixed bias voltage $V_B = 16$ V. From the probe sweep in Figure 11, the probe current at this bias voltage is dominated by I_e (collection of plasma electrons), and we may neglect the current due to photoelectrons emitted by the probe. Probes 3 and 4 have a bias current $I_B = -150$ nA. With a photoelectron saturation current of -530 nA (Figure 1), they will stay at positive potentials V_3 and V_4 (compare equation (3)). The sweep also shows that the satellite potential V_S is positive, and as V_B is +16 V in normal operations, the potential of probes 1 and 2, $V_{1,2} = V_S + V_B$ in the unperturbed plasma, is even higher. The photoelectron current to these probes may therefore be completely neglected (compare to Fig. 11 and to equation (3)). The system of equations (21) - (24), where the currents are given by (3), (6), and (25) and the parameters αn and T^* are empirically obtained from some nearby probe sweep, can now be reduced to three coupled nonlinear ordinary differential equations for V_3, V_4, and V_S:

$$C_E\frac{dV_S}{dt} - (C_E + C_P)\frac{dV_3}{dt} - (1 + \frac{\delta n_3}{n_0})\frac{V_3}{R_e} = \\ = \quad (1 + \frac{\delta n_3}{n_0})\frac{T^*}{R_e} - I_{ph,0}\exp(-V_3/T_{ph}) + C_E\frac{d\Phi_3}{dt} + I_B \tag{31}$$

$$C_E\frac{dV_S}{dt} - (C_E + C_P)\frac{dV_4}{dt} - (1 + \frac{\delta n_4}{n_0})\frac{V_4}{R_e} = \\ = \quad (1 + \frac{\delta n_4}{n_0})\frac{T^*}{R_e} - I_{ph,0}\exp(-V_4/T_{ph}) + C_E\frac{d\Phi_4}{dt} + I_B \tag{32}$$

$$(DC_P + C_E)\frac{dV_S}{dt} - C_E\frac{dV_3}{dt} - C_E\frac{dV_4}{dt} = \\ = \quad D^2\, I_{ph,0}\exp(-V_S/T_{ph}) - (D^2\ \left[1 + \frac{\delta n_S}{n_0}\right] + 1 + \frac{\delta n_1}{n_0})\frac{V_S}{R_e} - D^2\ \frac{T^*}{R_e}(1 + \frac{\delta n_S}{n_0}) + \\ -\frac{T^* + V_B - \Phi_1}{R_e}(1 + \frac{\delta n_1}{n_0}) + C_P\frac{d\Phi_1}{dt} + C_E\frac{d\Phi_3}{dt} + C_E\frac{d\Phi_4}{dt} + 2I_B \tag{33}$$

where $R_e = T^*/I_{e0}$ denotes the unperturbed probe sheath resistance in the coupling to plasma electrons, which from (7) is

$$R_e = T^*/I_{e0} = \frac{1}{4\pi a^2 e\alpha n_0}\sqrt{2\pi m_e T^*/e}. \tag{34}$$

On Viking, voltage probes (3 and 4 in the circuit in Figure 9) operate at a bias current of -150 nA. This places them on a part of the probe curve which is dominated by photoelectron emission (compare to equation (3) and Figure 1) and has maximal steepness. Changes in V_3 and V_4 will therefore be small. Also, $C_E \ll D\,C_P + C_E$, so the last two terms on the LHS of (33) are negligible, and (33) is therefore almost decoupled from (31) and (32). Physically, this means that the satellite potential is effectively independent of the variations at the V-mode probes 3 and 4. The capacitive terms (LHS) in equation (33) will normally be small compared to the resistive terms on the RHS. Also, the variations in satellite potential are usually small compared to the probe potential variations, so the first terms on the LHS of (31) and (32) may often be neglected as well. Therefore, in many cases the system above reduces to one transcendental equation for the satellite, and one nonlinear ordinary differential equation for each of the voltage probes (3 and 4 in this case). In the numerical calculations in this paper, we have solved the full equations shown above in order to have a general method applicable to different phenomena in different environments. Numerical calculations using approximations as listed have only been used for checking the results.

The signals measured onboard and transmitted to the ground are $U_{34} = U_3 - U_4$ and $\delta I_1/I = (I_1 - I_{10})/I_{10}$, where I_{10} is the probe current in the unperturbed plasma. After solution of the system above, the measured quantities are given by (26) and (28) as

$$U_{34} = \Phi_3 - \Phi_4 + V_3 - V_4 \tag{35}$$

$$\frac{\delta I_1}{I} = \frac{\delta n_1}{n_0} - \frac{1}{V_{10}} \left[\Phi_1 + \frac{R_e C_P}{1 + \frac{\delta n_1}{n_0}} \frac{d}{dt}(\Phi_1 + V_S) \right] \tag{36}$$

where index 0 refers to the unperturbed plasma.

The above model for the SW measurements may be studied by approximative analytical methods or by numerical integration. As the probe current fluctuation can be up to 80 per cent, linearizing the equations is not always appropriate. We here solve the full equations (31) - (33) by numerical integration, using equations (29) - (30) to describe the SWs. Before sampling, the signal is low-pass filtered with a 3 dB damping point at half the sampling frequency (*Eriksson et al.*, 1995). The effects of these filters have been included in the numerical calculations.

The system to be solved includes a number of parameters for the SWs: ν_0, Φ_0, u, L, $\Delta\Phi$ and L'. For a symmetric SW, the last two parameters disappear, and four parameters remain. Figure 12 shows the result of modelling the measurement of a SW observed by Viking at UT 082538, July 31, 1986. The instrument sampled the signals U_{34} and $\delta I_1/I$ at 428 samples/s. The observed signals are shown as open circles in panels c and d. Good agreement between observed and modelled voltage variation (panel c) was found for parameter values $v = 20$ km/s, $L = 50$ m, and $\Phi_0 = 4$ V. To get good correspondence between measured and modelled probe current fluctuation (panel d), ν_0 was adjusted to 50 %. It is notable that this procedure results in a good modelling of the particular features of $\delta I_P/I_{P0}$ not originating from the assumed Gaussian density fluctuation (dashed curve). The origin of these spurious signals can be traced to the variation of the satellite potential, shown in the upper right panel, when the density depletion in the SW passes the satellite. As is seen from (28), the positive change in V_S adds to Φ_2, which is positive when the negative SW passes the satellite body. This adds a negative bipolar structure to the current, proportional to the negative derivative of $V_S + \Phi_2$, due to capacitive effects. A similar bipolar structure, somewhat smaller as V_S is constant here, is added to the main minimum in the probe current. However, the main minimum still gives a good representation of $\delta n/n$. To summarize, the measurement error for the potential of the SW is insignificant, while the error in the density fluctuation estimate is significant,

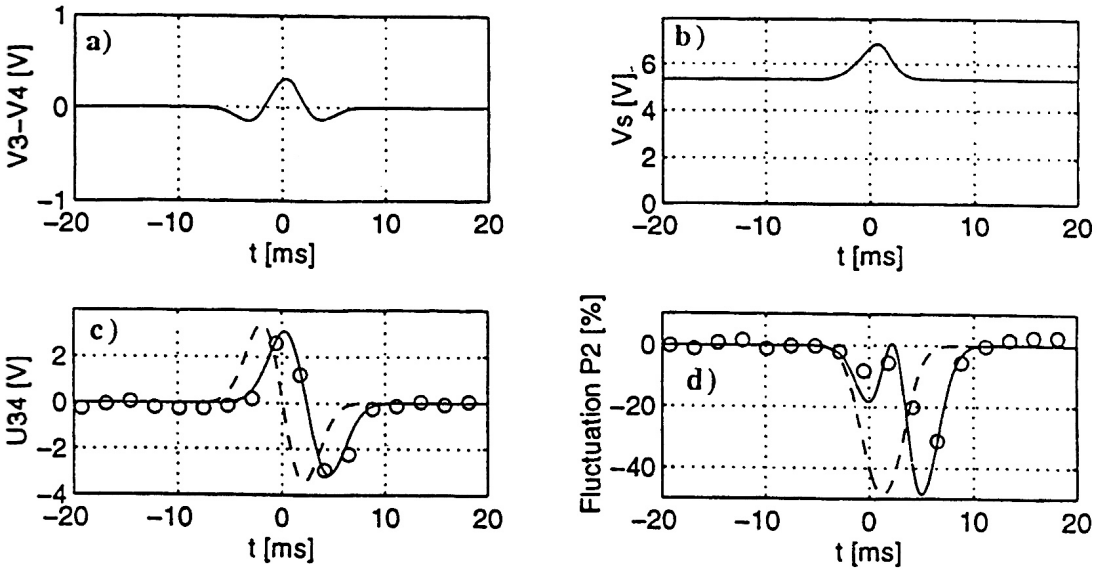

Figure 12: Simulation of a SW measurement.

although well understood. For further discussions of the SW measurements, the reader is refered to the report by *Eriksson et al.* [1995].

5 Sheath nonlinearities

5.1 Effects of sheath non-linearities on wave measurements

The probe curve is obviously not perfectly linear. The presence of nonlinearities implies that a perturbation of V_P, with a certain frequency results in a current response involving a spectrum of frequencies. For a sinusoidal perturbation, the principal effects may be sorted into rectification, which is the response at zero frequency, and the generation of harmonics. We will here concentrate on rectification. For sounding rockets, *Boehm et al.* (1994) have studied the rectification effect on electric field measurements, while *Ergun et al.* (1994) have considered the effect on density measurements. We will here consider measurements of solitary wave phenomena on Viking and Freja. In the Viking case, we investigate if the solitary wave structures discussed in Section 4.2 could possibly be signatures of wave packets, for example travelling Langmuir or lower hybrid cavitons, rather than of actual solitary pulses. For Freja, we consider the question if the probe current minima observed simultaneously with bursts of lower hybrid waves may be an effect of rectification of the waves rather than of density depletions.

5.2 Application: Can the solitary waves observed on Viking be rectified wave packets?

To answer this question, we will here study what signature a rectified wave packet would give in the Viking data.

In a thin plasma, such as encountered by Viking in SW regions (*Eriksson et al.*, 1995), the dominant nonlinearity in the probe equations is the photoelectron current. For probes in density mode, for which $V_P \gg T_{ph}$, the photoelectron current is small and the nonlinear effects are weak. In contrast, probes in voltage mode, which we concentrate on here, operate on the steep part of the probe curve, where the nonlinear photoelectron current completely dominates the current (compare Figure 11). For voltage probes, we may assume constant satellite potential, since the measured quantity is the voltage difference between two probes (equation (24)), and variations in V_S therefore do not affect the results. Neglecting I_e and I_i, equations (5), (21), and (23) yields

$$I_{ph}(V_P) + (C_P + C_E)\frac{dV_P}{dt} - I_B - C_E\frac{d\Phi_P}{dt} = 0. \tag{37}$$

If the perturbation amplitude is sufficiently small to keep $V_P > 0$, we get

$$I_{ph,0}\ \exp\left(-\frac{V_P}{T_{ph}}\right) - (C_P + C_E)\frac{dV_P}{dt} = I_B + C_E\frac{d\Phi_P}{dt}. \tag{38}$$

This equation is readily analyzed with a standard two time scales technique. The ansatz

$$V_P = V_{(0)} + V_{(1)}, \tag{39}$$

where $V_{(0)}$ is the equilibrium probe potential for Φ_P constantly at zero, gives

$$I_B\left[\exp\left(-\frac{V_{(1)}}{T_{ph}}\right) - 1\right] - (C_E + C_P)\frac{dV_{(1)}}{dt} = C_E\frac{d\Phi_P}{dt}. \tag{40}$$

For a sinusoidal perturbation,

$$\Phi_P = \Phi\ \sin\omega t, \tag{41}$$

the perturbation ansatz

$$V_{(1)} = V_{lin} + V_{nl} \tag{42}$$

where $V_{nl} \ll V_{lin}$ yields the linearized equation

$$\frac{dV_{lin}}{dt} + \omega_0 V_{lin} = -\frac{C_E}{C_E + C_P}\frac{d\Phi_P}{dt} \tag{43}$$

with solution

$$V_{lin} = -\frac{C_E}{C_E + C_P}\frac{\omega}{\omega_0^2 + \omega^2}(\omega\ \sin\omega t\ +\ \omega_0\ \cos\omega t)\ \Phi, \tag{44}$$

where the characteristic angular frequency is

$$\omega_0 = \frac{I_B}{(C_E + C_P)T_{ph}}. \tag{45}$$

This gives a characteristic frequency $f_0 = \omega_0/2\pi \approx 1$ kHz for $T_{ph} = 1$ eV. Expanding (40) to second order in V_{lin} and first order in V_{nl}, we get

$$V_{nl} = \frac{1}{2}\frac{1}{T_{ph}}V_{lin}^2 + \frac{1}{T_{ph}}V_{lin}V_{nl} - \frac{1}{\omega_0}\frac{dV_{nl}}{dt}. \tag{46}$$

For a small perturbation, the second term on the RHS may be neglected. To find rectification effects, we want to find the average value of V_{nl} over a wave period. The last term on the RHS does not contribute to the average, which is found to be

$$V_{nl}^{av} = \frac{\omega}{2\pi}\int_0^{2\pi/\omega} V_{nl}\ dt = \frac{1}{4}\left(\frac{C_E}{C_E + C_P}\right)^2 \frac{\omega^2}{\omega_0^2 + \omega^2}\frac{\Phi^2}{T_{ph}}. \tag{47}$$

If a high frequency wave is modulated by a low frequency envelope, this modulation will show up in our measured signal, where frequencies above a few hundred hertz are filtered away, as a low frequency signal of amplitude V_{nl}^{av}. It follows from (35) that this will be the real observed error in the measured voltage signal. A wave of amplitude 25 mV/m and wavelength much longer than the boom length of 40 m may induce a 0.1 V amplitude in potential between probe and satellite. If the frequency is 1 kHz and $T_{ph} = 1$ eV, we get $V_{nl}^{av} \approx 1$ mV. Higher wave amplitudes will give higher values of V_{nl}^{av}, but then the perturbation approach breaks down and (47) does not provide quantitatively correct results.

The most important feature of the rectification effect described by equation (47) is that V_{nl}^{av} is strictly positive. This is a perturbation result, but by considering its physical origin it becomes clear that it is valid also for high amplitude waves. Consider a sphere with a bias current of 150 nA. A fluctuation of potential in the plasma couples to the probe potential as described to zeroth order by (44). It is clear from the probe curve shown in Figure 11 that if we compare a small negative and a small positive perturbation of V_P from its equilibrium value, the effect on the probe current is largest for the negative perturbation because of the nonlinearity of the probe curve. For a sinusoidal perturbation, the average of the current response during one period will then be negative. Therefore, variations in probe potential result in a net decrease of the already negative probe current. However, the average current must stay constant, as it is constrained by the bias voltage. In order to keep the current constant, the average probe potential must increase. This is exactly the opposite of the case studied by *Boehm et al.* (1994) who considered probes at negative potential in the nightside ionosphere. The dominating nonlinearity in their case is the exponential

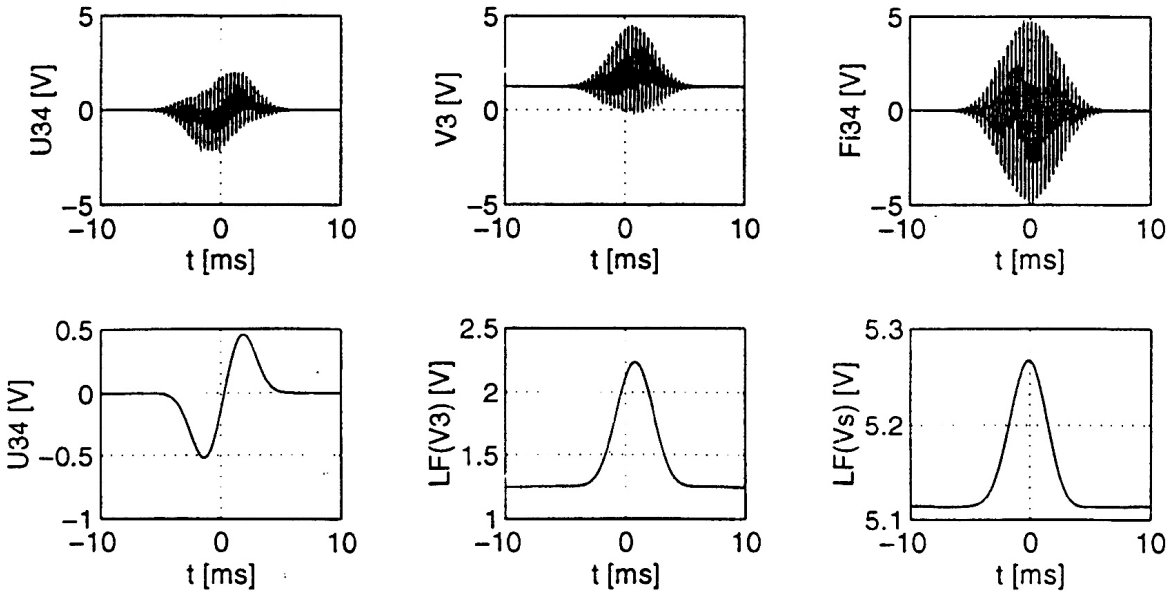

Figure 13: Simulation of rectification of the voltage signal for a hypothetical wave packet on Viking.

term in (6), which has a second derivative of the opposite sign compared to our case. Consequently, they concluded that the rectification effects in their case should appear as negative voltage offsets.

Considering equation (26), it is clear that the effects of an external potential variation Φ and a variation of the probe potential are equivalent for voltage measurements with double probes. Therefore, the SWs observed on Viking, which all have the appearance of a local potential minimum (compare to Figure 6 of *Mälkki et al.* (1993)) cannot be signatures of rectified wave packets.

Numerical solution of the probe equations (21) – (24) of the same character as in Section 4.2 may be applied to this problem as well. For the simulation, we have modified the set of equations (31) – (33) by removing their restriction to positive probe potentials and using the full expressions (3) and (6). Equation (30) for the perturbation was replaced by

$$\Phi(z,t) = \Phi_0 \exp\left(-\left[\frac{z-ut}{L}\right]^2\right) \cos\left(2\pi\left[\frac{z}{\lambda} - ft\right]\right) \tag{48}$$

to represent a wave packet with group velocity u and phase velocity $f\lambda$ along the magnetic field. The density fluctuation was put to zero as we focus the interest on rectification. We have used the same values of plasma parameters, boom angles, structure speed u and extent L as for the SW in Figure 12, but Φ_0 was put at 3 V, and the frequency and wavelength of the wave is $f = 3$ kHz and $\lambda = 100$ m, respectively. This does not necessarily represent any wave mode actually observed on Viking, but is chosen as an example of rectification effects. The upper row in Figure 13 shows, from left to right, the measured signal U_{34}, the potential of one of the probes V_3, and the potential difference in the plasma between the locations of probes 3 and 4, which is the input to the simulation and what should have been observed in U_{34} if the measurement was ideal. Effects of the sheath nonlinearities are clearly seen in U_{34} and V_3. The bottom row of the figure shows low-pass filtered versions of the signals U_{34}, V_3, and the satellite potential V_S to highlight the rectification effects. As expected, V_P and V_S show positive excursions, and a bipolar structure is seen in U_{34}, with opposite sign compared to the one which is observed in a solitary wave measurement (compare

Figure 12).

For the current probes, rectification effects in the probe sheath will be small, as noted above. However, the circuit also includes the nonlinear satellite sheath, which may be a more efficient rectifier. A simulation including both probe and satellite sheaths have been performed, and resulted in a bipolar rectified structure in the probe current, with an amplitude of 0.5 % for the parameters used for the voltage rectification signal above. The reason for a bipolar structure to form is clear. As was seen above, rectification causes the satellite potential to move, about 0.15 V in this example (Figure 13). For a density probe at fixed bias, the probe voltage will vary accordingly. As the probe is mainly capacitively coupled to the plasma, a bipolar signature results in the probe current due to the unipolar rectified satellite potential variation seen in Figure 13. Further discussions on rectification in the satellite sheath is found in the Freja application in Section 4.2. Here, we just conclude that neither the voltage nor the probe current signature of the observed SWs on Viking can be due to rectification of hypothetical wave packets. The interpretation of these phenomena as solitary wave pulses is confirmed.

5.3 Application: Freja observations of small-scale density depletions with enhanced lower hybrid wave power

Figure 14 shows an example of Freja observations of so called lower hybrid cavities, LHCs (*Eriksson et al.*, 1994; *Dovner et al.*, 1994). The observational signature of these is an enhanced voltage fluctuation around and above the lower hybrid frequency (typically a few kHz), coincident with a probe current decrease with a width of around 10 ms. The minimum in the probe current has been interpreted as a density depletion. We will here investigate if it is possible to explain it in terms of rectification of the observed waves instead (*Ergun et al.*, 1994). This is a question of highest interest, since almost all attempts to understand the physics of these structures concentrate on the coupling of lower hybrid waves and density depletions (*Robinson et al.*, 1995; *Singh*, 1994; *Pécseli et al.*, 1994).

5.3.1 Rectification in probe sheaths

First studying the probe sheaths, we may write the probe characteristic locally around the point of operation of a density probe as suggested by (16). Neglecting variations of V_S, equation (21) implies that the perturbation of the probe potential will be coupled to the electric field in the plasma by $\delta V_P \approx -\delta\Phi_P$. In the case of no density perturbation, we then have

$$\frac{\delta I_P}{I_{P0}} = -\left(\frac{1}{RI_{P0}} + \frac{C_P}{I_{P0}}\frac{d}{dt}\right)\ \delta\Phi_P + a_2\left(\delta\Phi_P\right)^2 + ... \tag{49}$$

Considering a perturbation of the form

$$\delta\Phi_P(t) = \Phi_0(t)\ \sin\ 2\pi f t \tag{50}$$

where the amplitude $\Phi_0(t)$ varies on a timescale much longer than the wave timescale,

$$\frac{1}{\Phi_0}\frac{d\Phi_0}{dt} \ll 2\pi f, \tag{51}$$

we have

$$\frac{\delta I_P(t)}{I_{P0}} = -\left[\frac{1}{R}\sin\ 2\pi f t + 2\pi f C_P\ \cos\ 2\pi f t\right]\Phi_0(t) - \frac{1}{2}a_2\Phi_0^2(t)\cos\ 4\pi f t + \frac{1}{2}a_2\Phi_0^2(t). \tag{52}$$

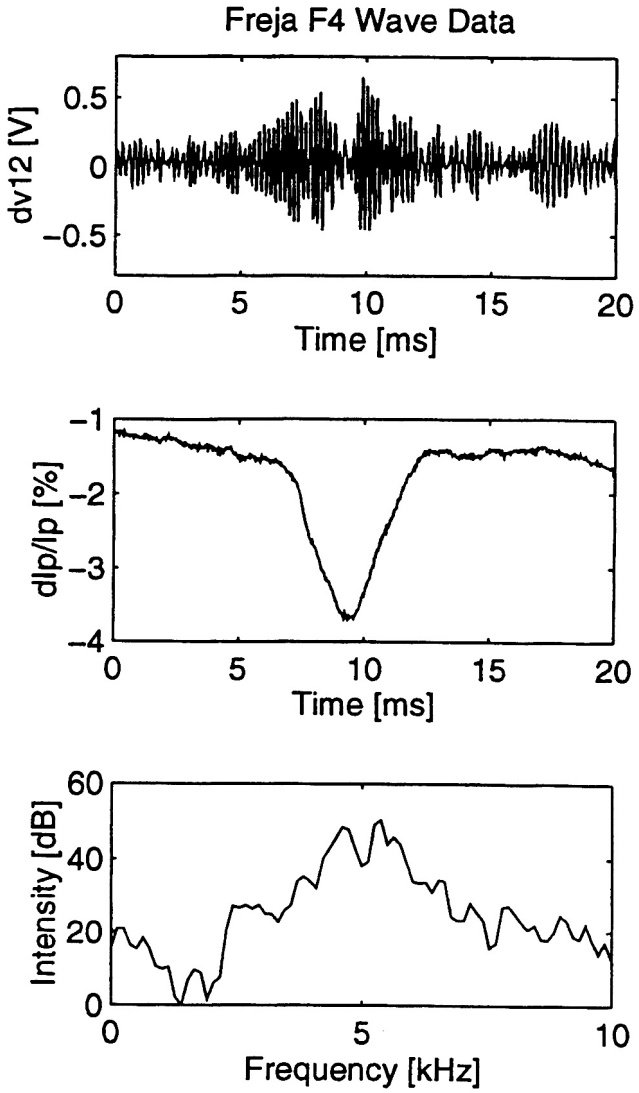

Figure 14: LHC observed by Freja on May 2, 1994, orbit 7580. Time is relative to UT 201319.499.

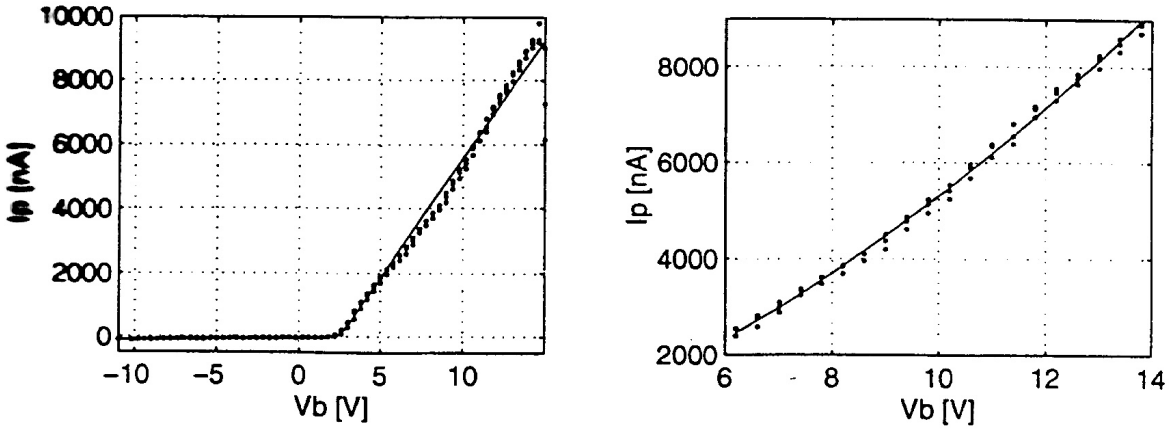

Figure 15: Left panel: Langmuir probe sweep recorded on Freja orbit 7580, May 2, 1994, at UT 201539, in the vicinity of the LHC in Figure 14. Fitting parameters using expressions in Section 2.3: $\alpha n = 1550$ cm^{-3}, $T^* = 0.4$ eV, $\beta n = 500$ cm^{-3}, $m^* = 1$ u, $V_S = -2.9$ V. Right panel: a blowup of the same sweep around the normal point of operation of density probes ($V_B = 10$ V), and a quadratic least squares fit to this part of the curve.

The term in the square brackets is a linear term at the fundamental frequency. The next term is a nonlinear harmonic, and the last term is the nonlinear low-frequency signal, which is our chief interest here.

A burst of oscillations of the form seen in Figure 14 may reasonably be described as a carrier wave with $f = 5$ kHz with an amplitude modulation $\Phi_0(t)$ with maximum value $\Phi_M = 0.5$ V. We wish to point out that effects of finite wavelength are not important to us here. Our aim is to model the voltage between a density probe and the satellite, not to determine the real electric field in the plasma. Using the measured voltage fluctuations between two probes 21.2 m apart, which is the signal shown at top of Figure 14, can, in the case of long wavelengths, make us overestimate the potential variation between the satellite and a density probe at a 5.6 m boom, but will otherwise not introduce any significant errors.

At left in Figure 15, a probe characteristic recorded close to the LHC observations in Figure 14 is shown. A quadratic least squares fit to points in the interval $V_B \in [\,6\text{ V},\ 14\text{ V}\,]$ in the sweep, shown at right in Figure 15, yields parameter values $R = 1.2$ MΩ, $a_2 = 5.4 \cdot 10^{-3}$ V^{-2}, and $I_0 = 5.3$ μA. Using $C_P = 14$ pF (Section 3.4), we find that the maximum amplitude of the fundamental oscillation in (52) is around 8 %, while the nonlinear terms have amplitudes below 0.1 %. The wave fluctuations at frequencies f and $2f$ are filtered away by a low-pass filter with 3 dB damping point at 1.3 kHz, and cannot be seen in the data. Only the rectified signal $\frac{1}{2}a_2\Phi_0^2(t)$

remains, with a maximum magnitude around 0.1 %, which obviously is far below what is needed to cause the observed probe current fluctuation. Moreover, it has the sign of an increase, not a decrease, of the probe current.

To explain the 3 % decrease in the probe current seen in Figure 14 in terms of rectification effects with the observed electric field, we would have to increase the value of a_2 by a factor of fifty. As a_2 is proportional to the second derivative of the probe characteristic (equation (13)), this would yield an unrealistic probe curve. The origin of the positive sign of a_2 is quite unclear, as it is not readily interpreted in terms of simple theory (equations (3), (6), and (10)). Most likely, it is an artefact of the plasma conditions changing during the time of the sweep. Values of a_2 of the same order are commonly found in other probe sweeps, also with opposite sign. Any real, consistently occuring nonlinearities in the probe characteristic must be smaller than the observed a_2 value, unless changing plasma conditions and spin modulation effects always act to balance the nonlinearity, which is most unlikely. We may note that the value of a_2 from the photoelectron current (3), which is the only nonlinear current term in this case, is $|a_2| \lesssim 10^{-5}$ V^{-2}.

5.3.2 Variations in satellite potential

Above, we showed that rectification in probe sheaths is not sufficient to cause observed probe current fluctuations. However, the probe current closes through the satellite and its sheath, which is another nonlinear element in the circuit. An electric field in the plasma causing a potential difference $\delta\Phi_P$ between satellite and probe will cause variations of the satellite potential V_S as well as of the probe potential V_P. From simple area considerations (equation (25), δV_S may be thought to be much smaller than δV_P, and it is thus tempting to rule out rectification in the satellite sheath. For the Viking observations of electric field signatures in tenuous plasma studied above (Section 4.2), the satellite potential was higher than the (voltage) probe potential, and the nonlinearities in the satellite sheath therefore weaker than the probe sheath nonlinearities. Also, the impedance in the coupling to the plasma was much lower for the satellite than for the probe. Finally, for the voltage probes studied in Section 4.2, variations in satellite potential are of limited interest, since V_S cancels in the measurement of voltage between two probes (equation (24)).

In contrast, for density probe measurements, variations of V_S are important, as can be seen from (28). For the dense plasma encountered by Freja, we normally have $V_S \lesssim 0$ in sunlight, as witnessed by probe sweeps and measurements of the floating ground potential (*Lindqvist et al.*, 1994). This has two important consequences. First, the probe curve is much more nonlinear near the satellite potential than near the potential of a density probe. Second, the satellite is on the high resistance ion and photoelectron dominated part of the probe curve, while the density probe is at the low resistance electron collection part. Taking the Freja sweep in Figure 15 as an example, the probe sheath resistances of these two branches are $R_{Pi} = (dI/dV)^{-1}_{V<0} \approx 190$ MΩ and $R_{Pe} = (dI/dV)^{-1}_{V>0} \approx 1.2$ MΩ. Assuming scaling by surface area, the satellite sheath resistance will be lower by a factor D^2, introduced in (25). D is the typical ratio of linear dimensions of the satellite and the probe. Freja has an approximate cylindrical shape, with radius 1 m and height 0.5 m, while the probes have radius 3 cm, so D could be expected to be around 15 – 20. We have used $D = 15$ in the calculations. In this case, we therefore have that the satellite sheath resistance R_{Si} is ~ 1 MΩ, which is about the same as for the probe sheath. Low frequency fields could therefore be distributed about equally over the probe and satellite sheaths. However, one should note that when the satellite is near $V_S = 0$ where the probe curve is nonlinear, and rectification effects are important, the resistance decreases from the R_{Si} value. Therefore, large fluctuations of V_S will anticorrelate with large rectification effects if the resistive coupling dominates. For the 5 kHz

waves in Figure 14, this is the case for the probe, as $1/2\pi R_{Pe}C_P \sim 10$ kHz if we use $C_P = 14$ pF as in Section 3.4. For the satellite, capacitive coupling, which will decrease the sheath impedance below the resistive value, will be important on the high resistance linear part of the probe curve, while resistive effects will dominate in the region where we have probe current nonlinearities, again giving the situation of large amplitudes in δV_S being anticorrelated to nonlinearities to rectify the fluctuations. Nevertheless, we cannot rule out the possibility that there may be sufficient fluctuations of V_S to cause significant rectification effects without further considerations.

5.3.3 Rectification in spacecraft sheath

From equations (3), (6), and (10) describing the different currents, it is clear that nonlinearities are most pronounced around $V_S = 0$. If floating without any bias currents or bias voltages to probes or other instruments, a satellite in darkness will normally aquire a slightly negative potential in order to balance electron and ion currents. In sunlight, photoelectrons add to the currents, and V_S can increase to near zero or positive values if the plasma is sufficiently thin. On the other hand, currents drawn by probes can, to some extent, balance this effect. For a satellite a few volts below zero, the most important nonlinearity in the spacecraft sheath should be the exponential in the electron current (6). *Boehm et al.* (1994) studied the effect of this nonlinearity on probe sheaths. For a probe floating at a potential $\sim -4T$, which is applicable in case of negligible photoemission, they found the expression

$$\Delta V = -T \ln \left[I_0(\delta V/T) \right], \tag{53}$$

where I_0 is the zeroth order modified Bessel function, for the rectified low frequency potential ΔV induced by a high frequency variation $\delta V \sin 2\pi f t$. This should be applicable to the satellite sheath as long as the perturbation is not large enough to make $V_{S0} + \delta V_S$ positive. In the opposite case of a very large fluctuation, we may instead approximate the satellite or probe characteristic by a piecewise linear function,

$$I(V) = \begin{cases} V/R_e, & V \geq 0 \\ \\ V/R_i \approx 0, & V < 0\,, \end{cases} \tag{54}$$

where V is the satellite potential plus some constant which may be found from the probe sweep as the point where the extrapolations of the linear parts (large negative and large positive potentials) cross. For $\delta V > |V_0|$, averaging over a period f^{-1} of the fluctuation yields

$$\Delta I \approx \frac{1}{\pi} \frac{\sqrt{\delta V^2 - V_0^2}}{R_e} \tag{55}$$

for $\delta V < |V_0|$ and zero otherwise. This increase in current must be balanced by a change of V_0 by an amount ΔV, given by the balance condition

$$\frac{\Delta V}{R_i} = -\frac{1}{\pi} \frac{\sqrt{\delta V^2 - (V_0 + \Delta V)^2}}{R_e}. \tag{56}$$

As $R_e \ll R_i$, we get

$$\Delta V \approx \delta V - V_0. \tag{57}$$

Hence, we may in the worst case have a rectified signal equal to the perturbation amplitude. This is of course an extreme case, not likely to be found in practice, but it shows the power of rectification effects in nonlinear sheaths.

In the example in Figure 14, we had voltage variations of 0.5 V. Assuming the extreme case of having all the wave voltage distributed over the satellite sheath, we could possibly get rectified low frequency signatures of the same amplitude. From (28), this could give a rectified signature $\Delta I/I \sim 5\,\%$. As ΔV_S is negative, the resulting signature in the probe current is a current minimum, which would be consistent with the observations if we underestimate the electric field by a factor of about 4. It is thus clear that it is not possible to rule out rectification effects on the basis of these semi-qualitative upper-limit considerations.

We therefore do a numerical simulation of the response of the probe-satellite-plasma system to a perturbation of the form (50) with Φ_0 a Gaussian. As the probe current is at the focus of our interest, we model the measurement system by a spherical probe in density (fixed bias voltage) mode and a presumably spherical satellite body. For this application, we do not neglect the photoelectron and ion currents to the density probe, as they, even though normally very small, are the sources of nonlinearity in the probe sheath. After elimination of V_P by (21) and (24), equations (15) and (25) in (22) yield

$$\begin{aligned} C_P\frac{d\Phi_P}{dt} - (C_S + C_P)\frac{dV_S}{dt} &= D^2 I_e(V_S) + D^2 I_i(V_S) + D^2 I_{ph}(V_S) + \\ + \quad I_e(V_S + V_B - \Phi_P) + I_i(V_S + V_B - \Phi_P) &+ I_{ph}(V_S + V_B - \Phi_P) + I_A \end{aligned} \tag{58}$$

where I_A is the current to the plasma from the satellite due to other sources, for example other probes and the cold plasma analyzer F3C (*Whalen et al.*, 1994), and the other currents are modelled by (3), (6), and (10). We have used I_A as a free parameter for moving the satellite potential, which is self-consistently determined in the numerical solution, around in order to maximize rectification effects. For the calculation of the probe current fluctuation, the full expression (27) was used.

Results of a numerical run with parameters from the sweep in Figure 15 and an amplitude of 0.5 V, corresponding to that seen in Figure 14, are shown in Figure 16. In order to maximize rectification effect, we have used a scaling factor D as low as 10. Also, we have put $C_S = DC_0$, where $C_0 = 3.3$ pF is the vacuum capacitance of a spherical probe, while keeping the experimentally determined value $C_P = 14$ pF in order to further increase the variations in satellite potential (calculations using $C_S = DC_P$ have also been made, showing less rectification). By using the parameter I_A, the satellite potential was adjusted until maximum rectification effects were found. As is seen in the figure, these are still quite weak. The low frequency variation in V_S was only about 7 mV, causing a current depletion of some 0.07 %, as expected from (28). Doubling the perturbation amplitude yields a rectified current decrease of 0.3 %, and an amplitude of 2.5 V yields about 1.5 % in rectified probe current decrease. However, such large potentials are clearly incompatible with Figure 14. The voltage could be underestimated by effects of capacitance division (Section 3.3), but even if the capacitance of the voltage probes was as low as C_0, this could only make us underestimate the voltage by less than a factor of two, since the input capacitance of probes 1 and 2, which were used for the voltage measurement in Figure 14, is 2.5 pF. We have also done calculations for T^* values of 0.1 eV and 2 eV, with corresponding changes in αn to keep a reasonable fit to the measured sweeps, without significantly changing the results.

Therefore, we conclude that the observed nonlinearities are too weak to explain the observed probe current fluctuations as effects of wave rectification, even though we have taken care to maximize the rectification. However, it is possible that there may exist nonlinearities not included in the model above. As mentioned in Section 3.2, numerical simulations by *Calder* (1984) and *Calder and Laframboise* (1985) have shown that for an electron collecting sphere, the capacitance decreases near the plasma resonance. It does not seem unreasonable to suspect that a similar effect may be found for an ion collecting probe or satellite near the ion plasma and lower hybrid frequencies.

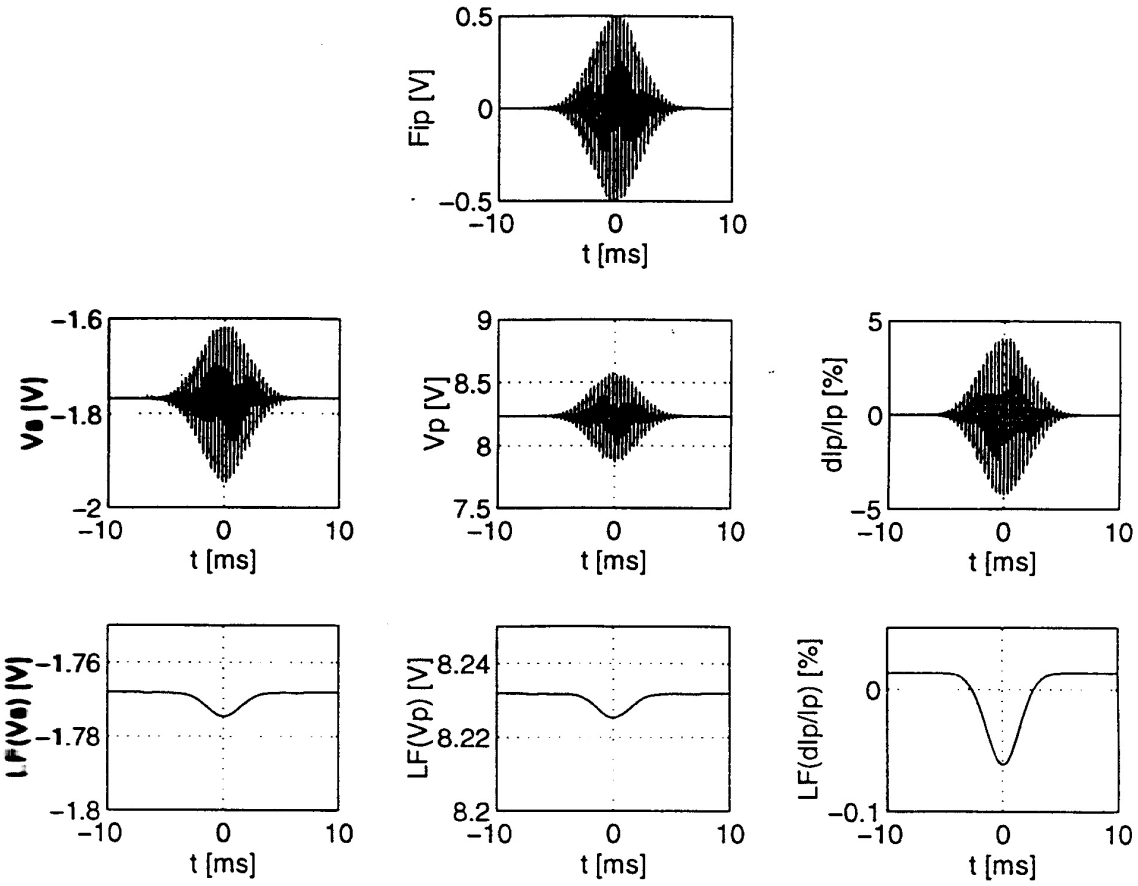

Figure 16: Simulation of Freja measurement of a lower hybrid wave packet without associated density depletion. Top panel: Model of observed voltage variation $\delta\Phi_P$. Center panels: Variations in V_S, V_P, and $\delta I_P/I_{P0}$ caused by the voltage in the top panel. Lower panels: Filtered versions of the signals in the center row to show rectification effects.

Also, the capacitance could change with changing sheath characteristics, and as these depend on the probe or satellite voltage, the problem becomes nonlinear. A study of such phenomena is far outside the scope of this paper, but we acknowledge their possible existence as a potential source of unknown rectification effects.

5.3.4 Observational evidence

The problem of establishing the importance of rectification effects in the LHC observations is to some extent accessible experimentally. From equation (52), we expect the rectified signal to closely follow the shape of the wave envelope. As is seen in Figure 14 and in numerous other LHC observations as well, this is rarely the case. This cannot be explained as a filter effect, since the filtering of the probe current signal at 1.3 kHz does not prohibit the reproduction of some details of the wave envelopes.

The use of multiple density probes also gives a possibility to identify rectification effects. If the observed probe current minima are due to density depletions at rest with respect to the plasma, the time difference Δt between their detection by two density probes will be related to the spacecraft velocity $\mathbf{v}_{sat}$ and the probe separation vector $\mathbf{d}$ by $\Delta t = \mathbf{d} \cdot \mathbf{v}_{sat}/v_{sat}^2$ (this is the time domain equivalent to the phase-frequency relation in the cross spectrum discussed in Section 3.4). However, if the current minimum is the result of rectification of the electric field, the corresponding result will depend on the characteristics of the modulation. If the width of the envelope of the wave field is small compared to the boom length, the voltage difference between probe and spacecraft will be maximum when the packet passes any of them. In case the rectification effect is most pronounced in the probe sheaths, this will give rectified signatures in the probe current when the structure passes the probes, which is the same result as the density fluctuation gives. If rectification in the satellite sheath is most important, the minimum in the probe current will be seen simultaneously in both probe current signals, when the structure passes the satellite. However, in our case, the spatial dimension of the modulation is comparable to the boom separation, and in this case the voltage between the probe and the spacecraft will have its maximum when the maximum of the envelope is halfway between them. Hence, the effective separation vector is $\mathbf{d}/2$ rather than $\mathbf{d}$, and the time delay Δt will be half the value it would be in the case of a density fluctuation causing the current decrease. Thus, it is in principle possible to distinguish between the two origins of the probe current minimum from a study of their characteristics. A preliminary analysis of this type (*Dovner et al.*, 1994) favours an interpretation in terms of density fluctuations. The evidence is not complete, as there is a certain spread in the data, which may be due to motion of the plasma or motion of the cavities with respect to the plasma. A further study, including plasma drift estimates using the DC electric field (F1) instrument on Freja, is needed for clarification.

We also note that we have LHCs observations at boom angles for the density probes with respect to the magnetic field at least within 15 degrees. We have not yet found any example at perfect alignment of boom and magnetic field, but this is probably due to the limited amount of data analysed from situations where the magnetic field is perpendicular to the satellite spin axis. If rectification was responsible, one should expect to find LHCs mostly at boom angles near 90°, assuming the wave electric field to be predominantly perpendicular. A systematic search for LHC observations made when the booms of the density probes are nearly parallel to the magnetic field is therefore of interest.

If rectification effects cannot explain the observed current minima, this does not automatically imply that they must be due to density depletions. There is also the possibility of temperature

fluctuations, mentioned in Section 3.1. A local increase of the electron temperature by about twice the $\delta I_P/I_{P0}$ value is also a possible explanation. In theory, it should be possible to use probes at different bias voltages to distinguish between density and temperature fluctuations, since equation (14) predicts a dependence on probe potential in the coupling of temperature fluctuations to the probe current. In practice, we have not succeeded in arriving at any conclusion using this method, due to the large spread of the data.

6 Conclusions

The general results found in this report can be summarized as follows:

1. The OML approximation together with measured probe sweeps is sufficient for the understanding of AC measurements when $r_P/\lambda_D > 1$, without any appeal to more detailed probe theory.

2. The probe capacitance can be estimated from a comparison of observed fluctuations in voltage and probe current. The result is consistent with estimates by other methods.

3. On Viking ($\sim 10,000$ km), the probe capacitance to the plasma is well approximated by the vacuum value. On Freja ($\sim 1,700$ km), the observed capacitance is much larger than the vacuum capacitance.

4. The satellite sheath is sometimes as important as the probe sheaths in causing spurious signals.

5. The nonlinearity in measured probe sweeps can be used to calculate rectification effects on measured signals, assuming that the displacement current is linear (described by a constant capacitance).

6. The simultaneous use of voltage and density probes is essential for the validation of either type of measurement.

We applied our discussion to some wave phenomena observed by the Viking and Freja satellites. For these specific phenomena we conclude that:

7. Probe current fluctuations with the same frequency as electric wave fields above the proton cyclotron frequency (Viking) and above the lower hybrid frequency (Freja) can be explained by capacitive and resistive coupling to the electric field.

8. The solitary pulses in voltage and density which are observed by Viking really are solitary waves. They cannot be due to travelling wave packets rectified in the probe sheath. Rather, they are solitary wave pulses of negative potential and decreased density.

9. Observed nonlinearities are too weak to cause the probe current minima observed by the Freja satellite in conjunction with lower hybrid wave bursts. The likely explanation for these minima is that they reflect real features in the plasma, presumably density depletions.

While the investigations above show that we have a good understanding of many aspects of probe behaviour, they also point at certain problem areas. Extended experimental investigations of probe and satellite capacitance are needed to understand the dependence of this quantity on plasma density, magnetic field strength, and photoelectron emission. Such investigations are possible by comparing fluctuations in the signals from voltage and current probes. In this context, it is particularly important to explore the possibility of nonlinearities in the displacement current, in order to fully understand rectification effects in wave measurements. Extended theoretical and numerical work is essential in this context, as this question may be hard to address experimentally.

We have seen in this report that spurious effects often contaminate measurements by electrostatic probes. However, we have also shown that it is possible to identify these errors in the data.

Essential in this is the availability of experimentally established probe sweeps, and the use of several probes, some in voltage mode and some in density mode. The signals from two or more probes in density mode can be compared, for example by cross spectral techniques, to identify effects of electric fields, and the comparison of voltage and probe current signals can be used to identify errors in any of them.

Acknowledgements

The help and cooperation of Anssi Mälkki is happily acknowledged, as is the language checking by Harley Thomas.

References

André, M., Dispersion surfaces, *J. Plasma Phys.*, *33*, 1–19, 1985.

André, M., H. Koskinen, G. Gustafsson, and R. Lundin, Ion waves and upgoing ion beams observed by the Viking satellite, *Geophys. Res. Lett.*, *14*, 463, 1987.

André, M., P. Norqvist, A. Vaivads, L. Eliasson, O. Norberg, A. I. Eriksson, and B. Holback, Transverse ion energization and wave emissions observed by the Freja satellite, *Geophys. Res. Lett.*, *21*, 1915–1918, 1994.

Benson, R. F., P. Bauer, L. H. Brace, H. C. Carlson, J. Hagen, W. B. Hanson, W. R. Hoegy, M. R. Torr, R. H. Wand, and V. B. Wickwar, Electron and ion temperatures - a comparison of ground-based incoherent scatter and AE-C satellite measurements, *J. Geophys. Res.*, *82*, 36–42, 1977.

Block, L. P., C.-G. Fälthammar, P.-A. Lindqvist, G. T. Marklund, F. S. Mozer, and A. Pedersen, Measurement of quasi-static and low frequency electric fields on the Viking satellite, Technical Report TRITA-EPP-87-02, Royal Institute of Technology, Stockholm, 1987.

Boehm, M. H., C. W. Carlson, J. P. McFadden, J. H. Clemmons, R. E. Ergun, and F. S. Mozer, Wave rectification in plasma sheaths surrounding electric field antennas, *J. Geophys. Res.*, *99*, 21361–21374, 1994.

Boström, R., H. Koskinen, and B. Holback, Low frequency waves and small scale solitary structures observed by Viking, in *Proc. 21st ESLAB Symposium (ESA SP-275)*, pp. 185–192, 1987.

Boström, R., G. Gustafsson, B. Holback, G. Holmgren, H. Koskinen, and P. Kintner, Characteristics of solitary waves and weak double layers in the magnetospheric plasma, *Phys. Rev. Lett.*, *61*, 82–85, 1988.

Brace, L. H., and R. F. Theis, Global empirical models of ionospheric electron temperature in the upper F-region and plasmasphere based on in situ measurements from the Atmosphere Explorer-C, ISIS-1, and ISIS-2 satellites, *J. Atmos. Terr. Phys.*, *43*, 1317–1343, 1981.

Calder, A. C., *Numerical simulation of the time-dependent sheath around an electrode in an isotropic collisionless plasma*, PhD thesis, York University, Toronto, Canada, 1984.

Calder, A. C., and J. G. Laframboise, Terminal properties of a spherical RF electrode in an isotropic Vlasov plasma: Results of a computer simulation, *Radio Sci.*, *20*, 989–999, 1985.

Carlson, M., The Langmuir probes on Freja, Technical Report UPTEC-94-07, Swedish Institute of Space Physics and Uppsala University, 1994.

Carlson, H. C., and J. Sayers, Discrepancy in electron temperatures deduced from Langmuir probes and from incoherent scatter data, *J. Geophys. Res.*, *75*, 4883–4886, 1970.

Chen, F. F., Electric probes, in *Plasma Diagnostic Techniques*, edited by R. H. Huddlestone and S. L. Leonard, pp. 113–200, Academic Press, New York, 1965.

Diebold, D. A., N. Hershkowitz, J. R. DeKock, T. P. Intrator, S.-G. Lee, and M.-K. Hsieh, Space charge enhanced, plasma gradient induced error in satellite electric field measurements, *J. Geophys. Res.*, *99*, 449–458, 1994.

Dovner, P.-O., A. I. Eriksson, R. Boström, and B. Holback, Freja multiprobe observations of electrostatic solitary structures, *Geophys. Res. Lett.*, *21*, 1827–1830, 1994.

Eliasson, L., M. André, A. I. Eriksson, P. Norqvist, O. Norberg, R. Lundin, B. Holback, H. Koskinen, H. Borg, and M. Boehm, Freja observations of heating and precipitation of positive ions, *Geophys. Res. Lett.*, *21*, 1911–1914, 1994.

Ergun, R. E., E. M. Klementis, G. T. Delory, J. P. McFadden, and C. W. Carlson, Plasma density observations during large-amplitude lower hybrid emissions, *EOS Trans.*, *75*, 552–553, 1994.

Eriksson, A. I., B. Holback, P. O. Dovner, R. Boström, G. Holmgren, M. André, L. Eliasson, and P. M. Kintner, Freja observations of correlated small-scale density depletions and enhanced lower hybrid waves, *Geophys. Res. Lett.*, *21*, 1843–1846, 1994.

Eriksson, A. I., A. M. Mälkki, P. O. Dovner, R. Boström, and G. Holmgren, A statistical study of auroral solitary waves and weak double layers. 2. Measurement accuracy and ambient plasma density, *J. Geophys. Res.*, *submitted*, 1995.

Fahleson, U., Theory of electric field measurements conducted in the magnetosphere with electric probes, *Space Sci. Rev.*, *7*, 238–262, 1967.

Fahleson, U., C.-G. Fälthammar, and A. Pedersen, Ionospheric temperaure and density measurements by means of spherical double probes, *Planet. Space Sci.*, *22*, 41–66, 1974.

Hilgers, A., B. Holback, G. Holmgren, and R. Boström, Probe measurements of low plasma densities with applications to the auroral acceleration region and AKR sources, *J. Geophys. Res.*, *97*, 8631–8641, 1992.

Holback, B., S.-E. Jansson, L. Åhlén, G. Lundgren, L. Lyngdahl, S. Powell, and A. Meyer, The Freja wave and plasma density experiment, *Space Sci. Rev.*, *70*, 577–592, 1994.

Holmgren, G., and P. M. Kintner, Experimental evidence of widespread regions of small-scale plasma irregularities in the magnetosphere, *J. Geophys. Res.*, *95*, 6015, 1990.

Hultqvist, B., The Swedish satellite project Viking, *J. Geophys. Res.*, *95*, 5749–5752, 1990.

Koskinen, H., P. M. Kintner, G. Holmgren, B. Holback, G. Gustafsson, M. André, and R. Lundin, Observations of ion cyclotron harmonic waves by the viking satellite, *Geophys. Res. Lett.*, *14*, 459, 1987.

Laakso, H., T. L. Aggson, and R. Pfaff Jr., Plasma gradient effects on double probe measurements in the magnetosphere, *Ann. Geophysicae*, *13*, 130–146, 1995.

LaBelle, J., and P. M. Kintner, The measurement of wavelength in space plasmas, *Rev. Geophys.*, *27*, 495, 1989.

Laframboise, J. G., Theory of spherical and cylindrical Langmuir probes in a collisionless, Maxwellian plasma at rest, Technical Report UTIAS report 100, Institute for Aerospace Studies, University of Toronto, 1966.

Laframboise, J. G., and J. Rubinstein, Theory of a cylindrical probe in a collisionless magnetoplasma, *Phys. Fluids*, *19*, 1900–1908, 1976.

Laframboise, J. G., and L. J. Sonmor, Current collection by probes and electrodes in space magnetoplasmas: A review, *J. Geophys. Res.*, *98*, 337–357, 1993.

Lindqvist, P., G. T. Marklund, and L. G. Blomberg, Plasma characteristics determined by the Freja electric field instrument, *Space Sci. Rev.*, *70*, 593–602, 1994.

Lundin, R., G. Haerendel, and S. Grahn, The Freja science mission, *Space Sci. Rev.*, *70*, 405–419, 1994.

Mälkki, A., *Studies on linear and non-linear ion waves in the auroral acceleration region*, PhD thesis, University of Helsinki, Finnish Meteorological Institute Contributions no. 11, 1993.

Mälkki, A., A. I. Eriksson, P.-O. Dovner, R. Boström, B. Holback, G. Holmgren, and H. E. J. Koskinen, A statistical survey of auroral solitary waves and weak double layers: 1. Occurrence and net voltage, *J. Geophys. Res.*, *98*, 15521–15530, 1993.

Marklund, C., L. G. Blomberg, P.-A. Lindqvist, C.-G. Fälthammar, G. Haerendel, F. Mozer, A. Pedersen, and P. Tanskanen, The double probe electric field experiment on Freja: Experiment description and first results, *Space Sci. Rev.*, *70*, 483–508, 1994.

Mott-Smith, H. M., and I. Langmuir, The theory of collectors in gaseous discharges, *Phys. Rev.*, *28*, 727–763, 1926.

Mozer, F. S., Analyses of techniques for measuring DC and AC electric fields in the magnetosphere, *Space Sci. Rev.*, *14*, 272–313, 1973.

Pécseli, H. L., K. Iranpour, Ø. Holter, J. Trulsen, B. Lybekk, J. Holtet, A. I. Eriksson, and B. Holback, Lower hybrid cavities detected by the Freja satellite, Technical Report UIO/PHYS/94-25, University of Oslo, 1994.

Pedersen, A., Solar wind and magnetosphere plasma diagnostics by spacecraft electrostatic potential measurements, *Ann. Geophysicae*, *13*, 118–129, 1995.

Robinson, P. A., A. Melatos, and W. Rozmus, Auroral lower-hybrid wave collapse?, *Geophys. Res. Lett.*, *in press*, 1995.

Rubinstein, J., and J. G. Laframboise, Theory of a spherical probe in a collisionless magnetoplasma, *Phys. Fluids*, *25*, 1174–1182, 1982.

Singh, N., Ponderomotive versus mirror force in creation of the filamentary cavities in auroral plasma, *Geophys. Res. Lett.*, *21*, 257–260, 1994.

Temerin, M., K. Cerny, W. Lotko, and F. S. Mozer, Observations of double layers and solitary waves in the auroral plasma, *Phys. Rev. Lett.*, *48*, 1175–1179, 1982.

Vago, J. L., P. M. Kintner, S. W. Chesney, R. L. Arnoldy, K. A. Lynch, T. E. Moore, and C. J. Pollock, Transverse ion acceleration by localized lower hybrid waves in the topside auroral ionosphere, *J. Geophys. Res.*, *97*, 16935–16957, 1992.

Whalen, B. A., D. J. Knudsen, A. W. Yau, A. M. Pilon, T. A. Cameron, J. F. Sebesta, D. J. McEwen, J. A. Koehler, N. D. Lloyd, G. Pocobelli, J. G. Laframboise, W. Li, R. Lundin, L. Eliasson, S. Watanabe, and G. S. Campbell, The Freja F3C cold plasma analyzer, *Space Sci. Rev.*, *70*, 541–561, 1994.